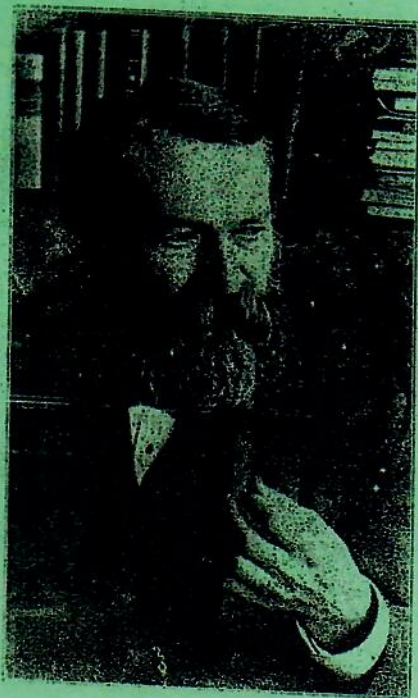


Palette of gravitoma(ch)gnetic effects

Jiří Bičák

Institute of theoretical physics, Charles University, Prague



Dr Ernst Much

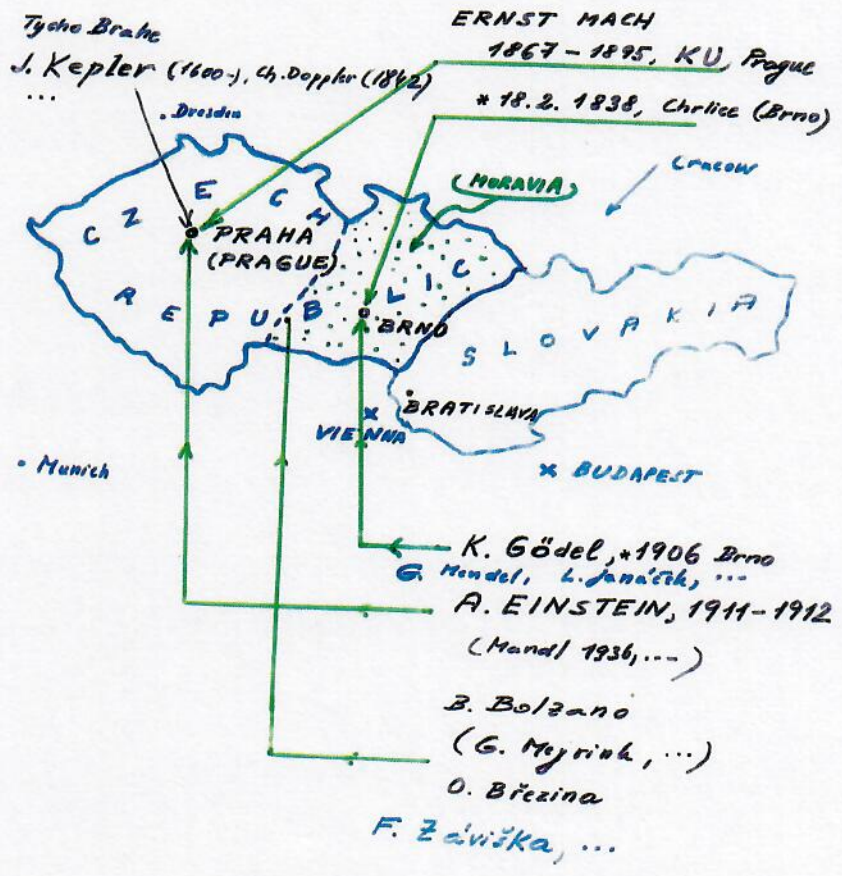
* 18 Feb 1838
in Chrlice (today part of Brno)
Moravia

+ 19 Feb 1916
Vaterstetten *)
Bavaria

last year 180 anniv.

**) (today part of Munich)*

"SPIRITUS LOCI"



" The highest philosophy of the scientific investigator is to bear with incomplete conception of the world *) and to prefer it to any apparently complete but inadequate conception * "

E. Mach, Science of Mechanics, p. 560

*) Euclidean barracks (kasárna, Kaserne) in absolute space

*) " The investigator must feel the need of... knowledge of the immediate connections... of the masses of the universe. There will hover before him .. an ideal insight into the principles of the whole matter, from which accelerated and inertial motion result in the same way "

E. Mach, S. of Mechanics.

3.

Gibt es eine Gravitationswirkung, die der elektrodynamischen Induktionswirkung analog ist?

Von

Prof. Dr. Einstein-Prag.

Die in der Ueberschrift aufgeworfene Frage kann in Anlehnung an einen übersichtlichen Spezialfall in folgender Weise formuliert werden. Es werde ein System ponderabler Massen betrachtet, bestehend aus der Kugelschale K mit homogen über die Kugelfläche verteilter Masse M und dem im Mittelpunkt dieser Kugelschale angeordneten materiellen Punkt P mit der Masse m. Wirkt auf den festgehaltenen materiellen Punkt P eine Kraft, wenn ich der Schale K eine Beschleunigung $\uparrow \Gamma$ erteile? Die folgenden Ueberlegungen werden uns dazu führen, eine solche Kraftwirkung als tatsächlich vorhanden anzusehen und uns die Grösse derselben in erster Annäherung ergeben.

force to hold P:

$$\frac{3 G m M \Gamma}{2 c^2 R}$$



solche Kraftwirkung als tatsächlich vorhanden anzusehen und uns die Grösse derselben in erster Annäherung ergeben.

1. Nach der Relativitäts-Theorie ist die träge Masse eines abgeschlossenen physikalischen Systems von dessen Energieinhalt in solcher Weise abhängig, dass ein Energiezuwachs des Systems um E die träge Masse um $\frac{E}{c^2}$ vergrössert, wenn c die Vakuum-Lichtgeschwindigkeit bedeutet. Bezeichnet man also mit M die träge Masse von K bei Abwesenheit von P, und mit m die träge Masse von P bei Abwesenheit von K, oder mit anderen Worten mit $M + m$ die träge Masse des aus P und K zusammen bestehenden Systems für den Fall, dass m sich in unendlicher Entfernung von K befindet, so folgt, dass die träge Masse des aus K und m bestehenden Systems, für den Fall, dass sich m im Mittelpunkt von K befindet, den Wert

$$M + m - \frac{k M m}{R c^2} \dots (1)$$

7. "Is There a Gravitational Effect Which Is Analogous to Electrodynamic Induction?"

[Einstein 1912e]

PUBLISHED July 1912

THE ANNALS OF PHYSICS

" STARRY NIGHT "

E. M.

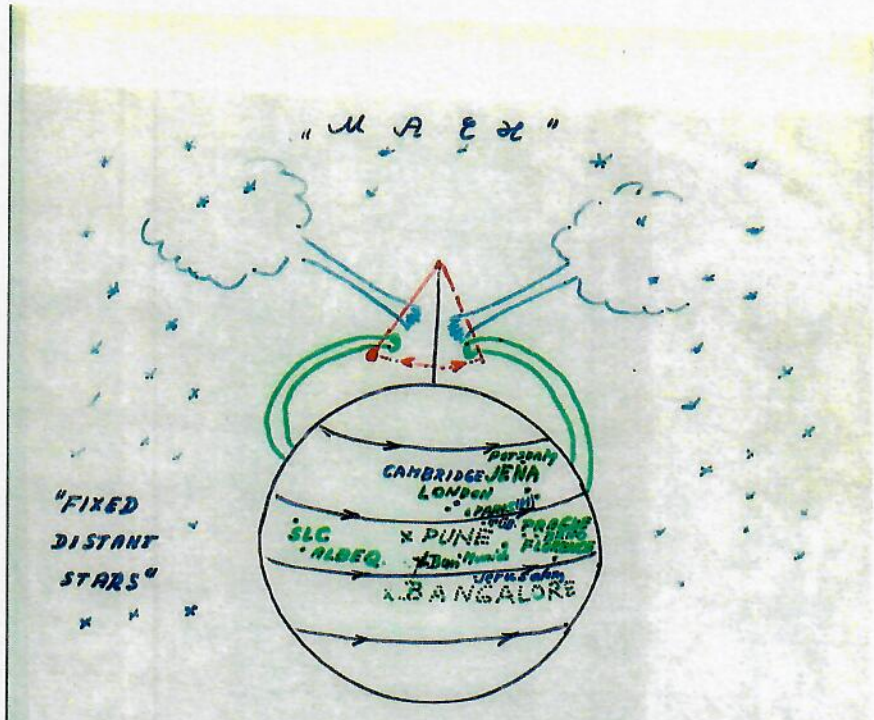
$$\omega (\text{drag}) = 2J_0 / r_0^3 \approx 229 \text{ millions} / \text{y}$$

PHYSICS ? ASTROLOGY ?

Gell-Mann

1. business	... 8. physicists	...
2. politicians	... 9. astrologists	20. astronomers
		mathematician

America's rating jobs:



GR : ω (drag) $\sim 2J_{\oplus} / r_{\oplus}^3 = 221$ milliarcsec/year

ELECTROMAGNETISM



Rotating charged sphere
 \rightarrow el. current \rightarrow magn. field \vec{B}

GRAVOMAGNETISM
 (in GR)



Rotating massive sphere
 \rightarrow mass-current \rightarrow gravitomagnetic field \vec{H}_g

GR drag - gravitomagnetism - given by

$$- 4 \vec{J} \times \vec{r} / r^3$$

← angular momentum of Earth



Frame drag at the Pole:

$$\omega = \frac{2J_{\oplus}}{r_{\oplus}^3} \dots = 221 \text{ milliseconds}$$

of arc per year

$$\left[\omega \sim \frac{GM_{\oplus}}{c^2 R_{\oplus}} \Omega_{\oplus} = 309 \text{ microarc/yr} \right]$$

Braginskij V.B., Polnarev A.G., Thorne K.S.

" Foucault Pendulum at the South Pole:

Proposal For an Experiment to Detect

the Earth's General Relativistic

Gravitomagnetic Field "

Phys. Rev. Lett. 53, 863 (1984)

- Bardeen-Petterson effect - neutron stars, black holes

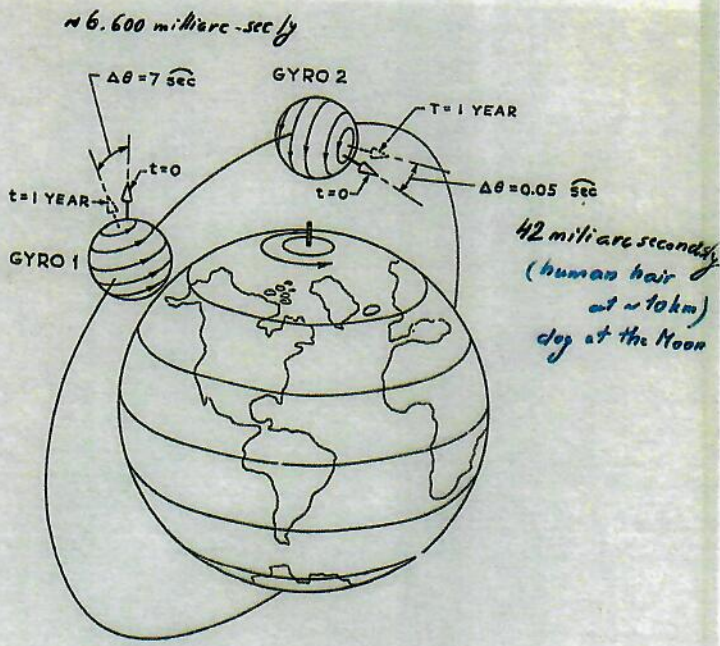


Figure 1

STANFORD GYRO EXPERIMENT

Idea: 1959 Launch: April 20, 2004
 First results: April 14, 2007 (APS, Jacksonville)
 Final results: End of 2007 **NO!**

\$35 mil.
↓
\$700 mil.

"GRAVITY PROBE B" (NASA)

Guide Star
IM Pegasi
(HR 8703)

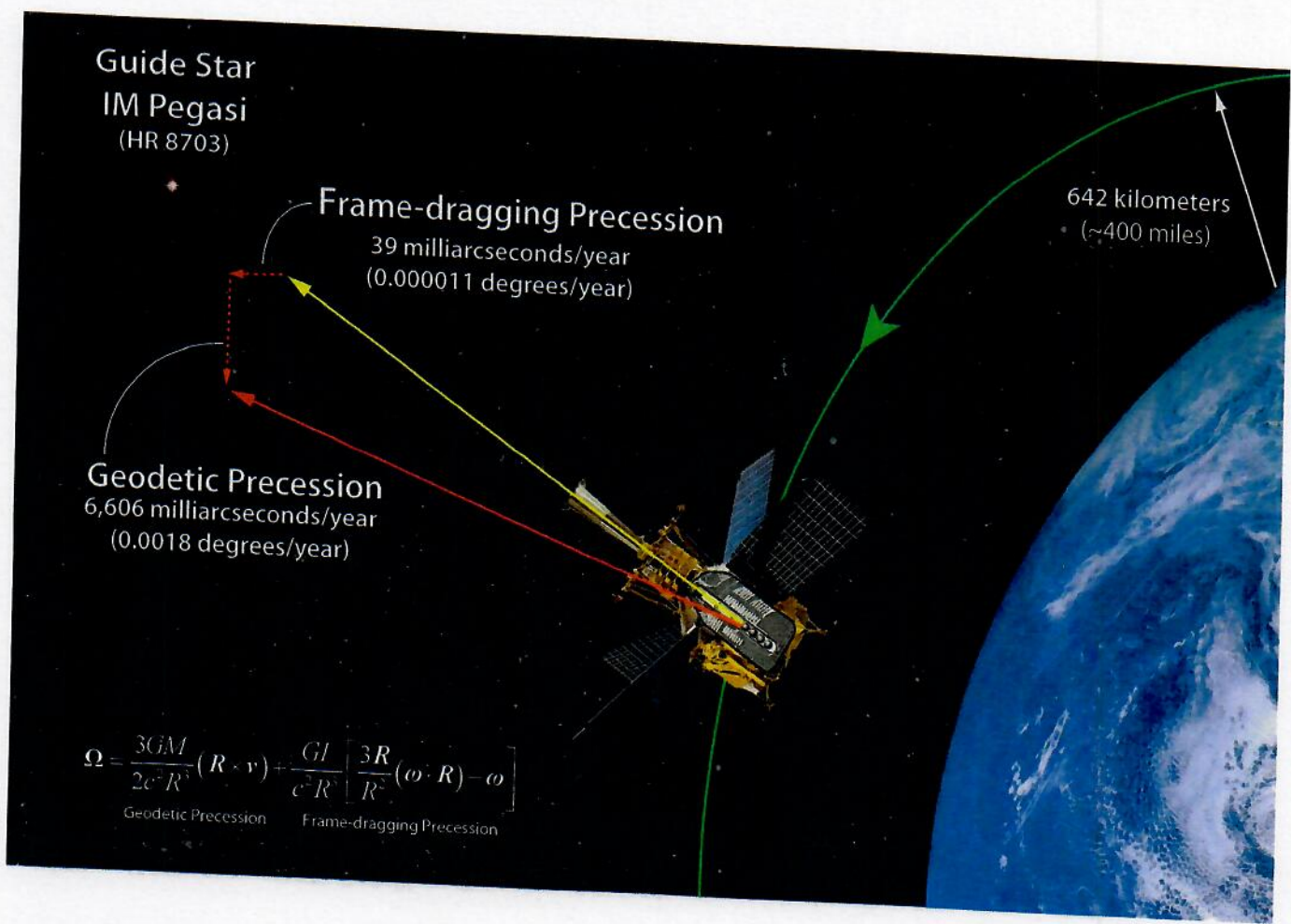
Frame-dragging Precession
39 milliarcseconds/year
(0.000011 degrees/year)

Geodetic Precession
6,606 milliarcseconds/year
(0.0018 degrees/year)

642 kilometers
(~400 miles)

$$\Omega = \frac{3GM}{2c^2 R} (R \cdot v) + \frac{GI}{c^2 R} \left[\frac{3R}{R^2} (\omega \cdot R) - \omega \right]$$

Geodetic Precession Frame-dragging Precession

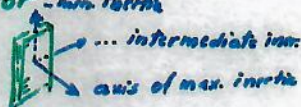


Mission Update - November 12, 2009

The accuracy of GP-B results has improved
17x since APS meeting in April 2007

In past 2.5 years modeling and removing
three Newtonian sources of error - non inertial

1) damped polhode motion



2) misalignment torques

torques on the gyros when spacecraft's
axis of symmetry not aligned with gyro's axes

3) roll-polhode resonance

All 3 effects due to "patch-effect"
anomalies

"while mechanically both rotor and housing
are exceedingly spherical, electrically they are not
patch charges arise from varying surface
electrical potentials in 'polycrystalline materials'

Analysis up to now:

COMBINED 4-GYRO RESULT GIVES STATISTICAL
UNCERTAINTY OF 14% (± 5 milliarcsec)
FOR THE FRAME DRAGGING

17 November 2015

The Gravity Probe B test of general relativity

G W F Everitt¹, B Muhlfeider¹, D B DeBra¹, B W Parkinson¹,
 J P Turneaure¹, A S Silbergleit¹, E B Acworth¹, M Adams¹,
 R Adler¹, W J Bencze¹, J E Berberian¹, R J Bernier¹,
 K A Bower¹, R W Brumley¹, S Buchman¹, K Burns¹,
 B Clarke¹, J W Conklin¹, M L Eglinton¹, G Green¹, G Gutt¹,
 D H Gwo¹, G Hanuschak¹, X He¹, M I Heifetz¹, D N Hipkins¹,
 T J Holmes¹, R A Kahn¹, G M Keiser¹, J A Kozaczuk¹,
 T Langenstein¹, J Li¹, J A Lipa¹, J M Lockhart¹, M Luo¹,
 I Mandel¹, F Marcelja¹, J C Mester¹, A Ndili¹, Y Ohshima¹,
 J Overduin¹, M Salomon¹, D I Santiago¹, P Shestopov¹,
 V G Solomonik¹, K Stahl¹, M Taber¹, R A Van Patten¹,
 S Wang¹, J R Wade¹, P W Worden Jr¹, N Bartel², L Herman³,
 D E Lebach⁴, M Ratner⁵, R R Ransom¹, I I Shapiro¹, H Small¹,
 B Stoozas¹, R Geveden¹, J H Goebel¹, J Horack¹,
 J Kolodziejczak¹, A J Lyons¹, J Olivier¹, P Peters¹, M Smith¹,
 W Till¹, L Wooten¹, W Reeve¹, M Anderson¹, N R Bennett¹,
 K Burns¹, H Dougherty¹, P Dulgov¹, D Frank¹, L W Huff¹,
 R Katz¹, J Kirschenbaum¹, G Mason¹, D Murray¹, R Farnley¹,
 M I Ratner⁵, G Reynolds¹, P Rittmuller¹, P F Schweiger¹,
 S Shehata¹, K Triebes¹, J VandenBeukel¹, R Vassar¹,
 T Al-Saud⁵, A Al-Jadaan⁵, H Al-Jibreen⁵, M Al-Meshari⁵ and
 B Al-Suwaidan⁵

¹ Stanford University, USA² NASA Marshall Space Flight Center, USA³ NASA Ames Space Flight Center, USA⁴ Lockheed Martin, USA⁵ King Abdulaziz City Science and Technology (KACST), Saudi Arabia

E-mail: francis@relgyro.stanford.edu, barry@relgyro.stanford.edu, ddebra@stanford.edu, thegstrad@gmail.com, johnturn@stanford.edu, alax.gleit@gmail.com, acworth@gmail.com, nea172@gmail.com, gyroron@gmail.com, wbencze@apple.com, john_berberian@icloud.com, robert.j.bernier@gmail.com, bower@relgyro.stanford.edu, brams@relgyro.stanford.edu, sbuchman@stanford.edu, kevin.tburns@nasa.gov, bence.d.clarke@nasa.gov, juconklin@ufl.edu, mike.eglington@gmail.com, paylord@att.net, gregory.gutt@gmail.com, gwoggg@gmail.com, gzh@stanfordalumni.org, huanxiao@gmail.com, mist_hej@yahoo.com, dhikins@relgyro.stanford.edu, theines.context@gmail.com, rnkahn@stanford.edu, mac@relgyro.stanford.edu, kozaczuk@stanford.edu, tom.langenstein@stanford.edu, je_qing88@yahoo.com, jipa@stanford.edu, jnstuck@sfu.edu, ming94305@yahoo.com, ilyamandel@chgtk.info, francis@gmail.com, jruenter@mit.edu, awele@relgyro.

GMB

**BLAIR
BUCKINGHAM**
EDITORS

RUFFINI
SERIES EDITOR

PROCEEDINGS OF THE FIFTH
**MARCEL GROSSMANN
MEETING ON
GENERAL RELATIVITY**

**D.G. BLAIR
M.J. BUCKINGHAM** EDITORS

REMO RUFFINI SERIES EDITOR

PROCEEDINGS OF THE FIFTH
**MARCEL GROSSMANN
MEETING ON GENERAL RELATIVITY**

PART B



PART B



World Scientific

only recall that each $F_{\mu\nu}$ can be expressed as a sum of two terms, one being proportional to B_θ , the magnitude of the component of the field asymptotically aligned with the hole's rotation axis, the other, B_r , being the magnitude of the component perpendicular to the axis. Following Christodoulou and Ruffini⁴ we define the magnetic (electric) lines of force as the lines tangent to the direction of the Lorentz force experienced by a test magnetic (electric) charge at rest with respect to the locally non-rotating frame. For the magnetic field lines this definition yields $dr/d\theta = -F_{\theta\phi}/F_{r\phi} = B_r/B_\theta$ and $dr/d\phi = F_{\theta\phi}/F_{r\theta} = B_r/B_\phi$.

In the case of the aligned field we can easily verify (by using $F_{\mu\nu}$ from Ref. 3) that the field lines lie on the surfaces of constant flux,

$$\Phi = \pi B_0 [\Delta + 2Mr\Sigma^{-1} (r^2 - a^2)] \sin^2\theta = \text{const.},$$

where

$\Delta = r^2 - 2Mr + a^2$, $\Sigma = r^2 + a^2 \cos^2\theta$; r, θ, ϕ are Boyer-Lindquist coordinates. The field lines, as constructed numerically, are in the case of the extreme Kerr black hole shown in Fig. 1. We can also define an "effective cross section" of the black hole, which is a circle determined by all field lines that eventually thread the horizon. Its radius at infinity can be shown to read $b = 2M(1 - a^2/M^2)^{1/2}$. This relation and Fig. 1 clearly show how the magnetic field is expelled from the horizon when the angular momentum of the hole increases. Analogously to the Reissner-Nordstrom case⁵, no field line of the asymptotically uniform magnetic field enters the horizon of an extreme Kerr black hole.

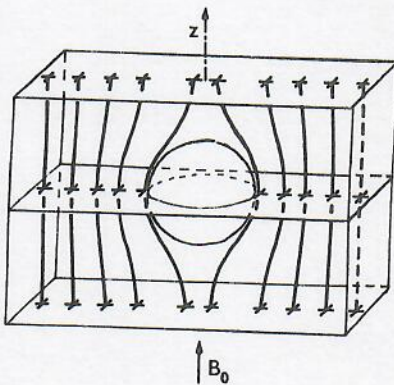
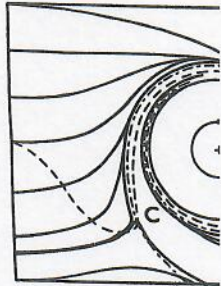


Fig. 1.

$B_\phi \neq 0$ and the field lines are dragged around the black hole. The lines, originally parallel to each other, are twisted, some of

6114
them threading the numerical perpendicular to $a/M=0.998$, as t above, are give coordinates ar corresponds to



a)



b)

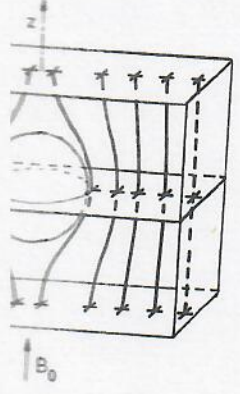
Fig. 2.

conducting sph caused by the hole and the of the electri

It that each $F_{\mu\nu}$ can be expressed as a sum of two terms, proportional to B_0 , the magnitude of the component of the asymptotically aligned with the hole's rotation axis, the being the magnitude of the component perpendicular to the rotation axis. Following Christodoulou and Ruffini⁴ we define the (electric) lines of force as the lines tangent to the of the Lorentz force experienced by a test magnetic charge at rest with respect to the locally non-rotating frame. The magnetic field lines this definition yields $dr/d\theta = B_r/B_\theta$ and $dr/d\phi = F_{\theta\phi}/F_{r\theta} = B_r/B_\phi$. In the case of the aligned field we can easily verify (by comparison with Ref. 3) that the field lines lie on the surfaces of constant r, θ ,

$$r^2 = \pi B_0 [\Delta + 2Mr\Sigma^{-1}(r^2 - a^2)] \sin^2\theta = \text{const.},$$

where $\Sigma = r^2 + a^2 \cos^2\theta$; r, θ, ϕ are Boyer-Lindquist coordinates. The field lines, as constructed numerically, are in the extreme Kerr black hole shown in Fig. 1. We can define an "effective cross section" of the black hole, which is determined by all field lines that eventually thread the horizon. Its radius at infinity can be shown to read $b = 2M(1 - a^2/M^2)^{1/2}$. This relation and Fig. 1 clearly show how the magnetic field is expelled from the horizon when the angular momentum of the hole increases. Analogously to the Reissner-Nordstrom case⁵, no field line of the asymptotically uniform magnetic field enters the horizon of an extreme Kerr black hole.



The structure of an asymptotically non-aligned field is much more complicated. In this case the field lines are dragged around the black hole. The field lines, which are initially parallel to each other, are twisted, some of

them threading the horizon even in the numerical construction of the field lines perpendicular to the rotation axis. The field lines, for $a/M=0.998$, as they look in the equatorial plane, are given in Fig. 2. The coordinates are wound up around the hole, which corresponds to the projection of the field lines on the equatorial plane.

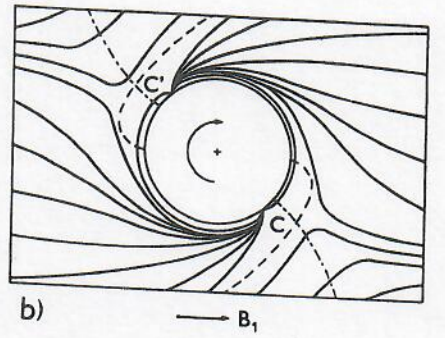
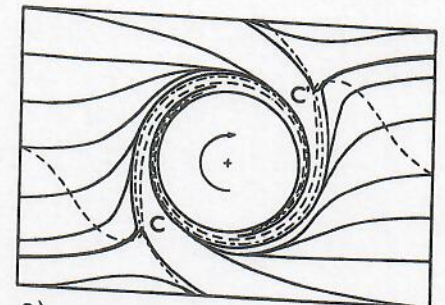
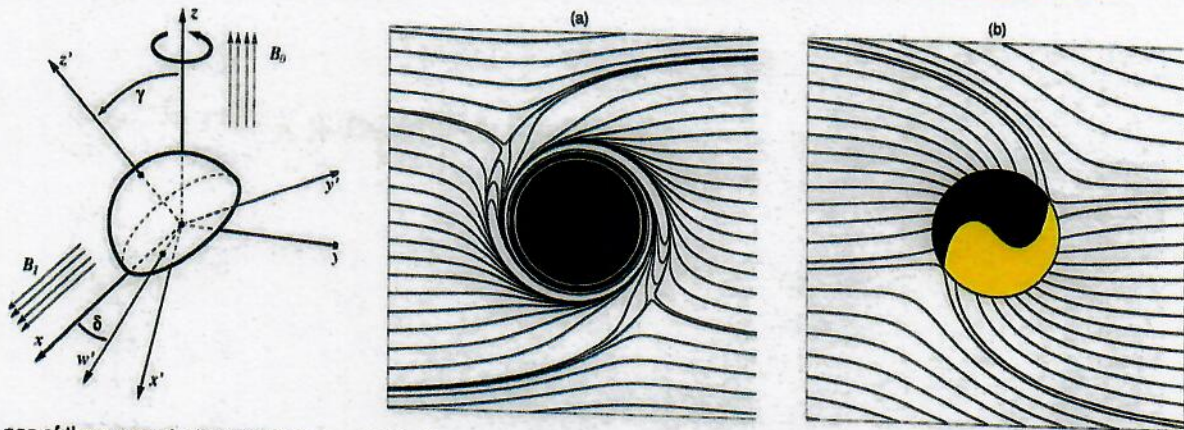


Fig. 2.

conducting sphere rotating in a uniform magnetic field. The field lines are caused by the gravitomagnetic interaction of the rotating black hole and the external magnetic field. The field lines of the electric field lines will be perpendicular to the magnetic field lines.

embe
Thor
ingc
do i
poin
by
curv
poin
vani
appe
to t
line:
Schw
field
lines
the
rotat
appr
bound
extre
Su
field
magne
the
quadr

on-axisymmetric fields – asymptotically uniform non-aligned fields

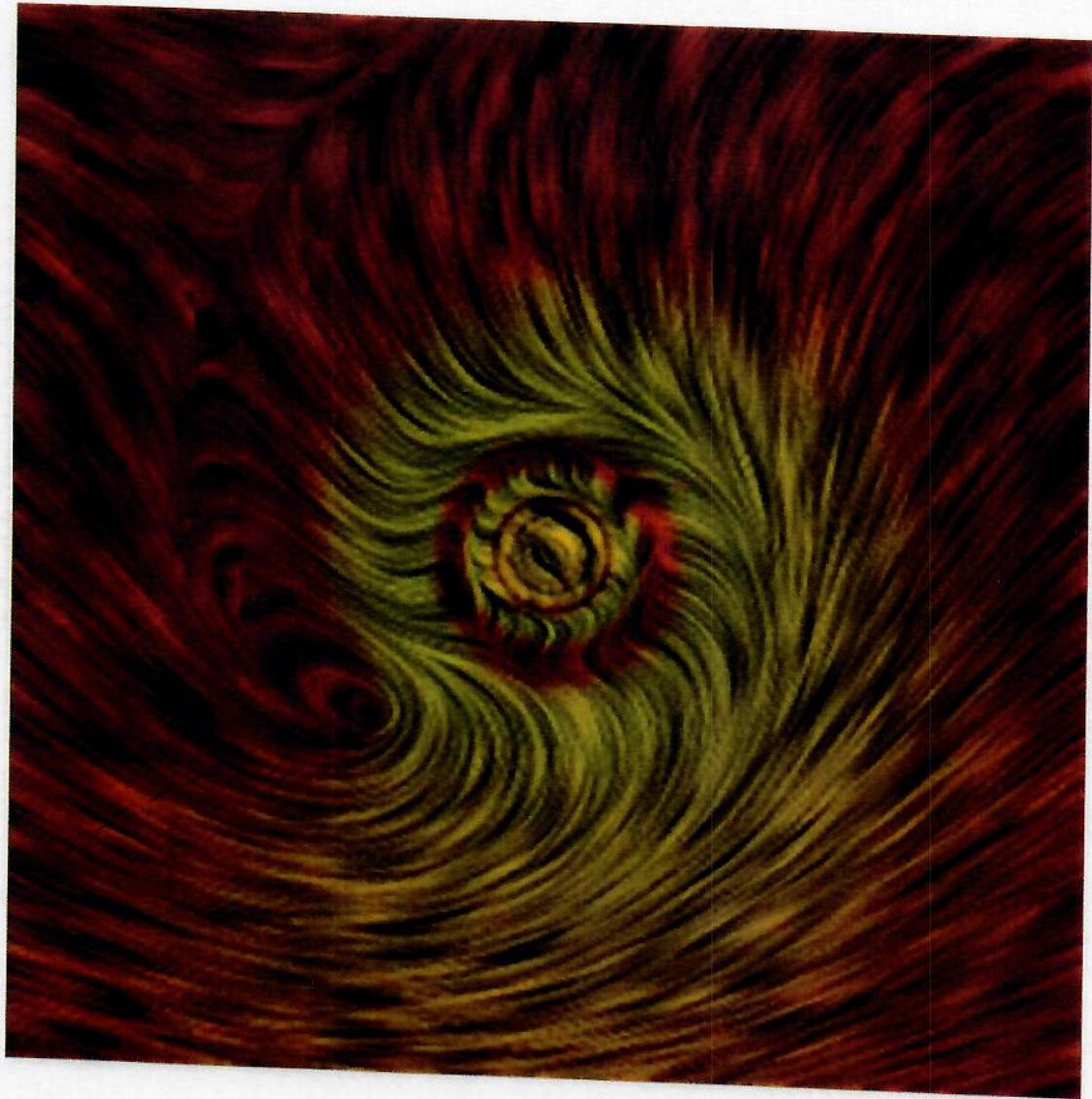


Lines of the magnetic field which is asymptotically uniform and perpendicular to the rotation axis. The equatorial plane is shown as viewed from top, i.e. along the rotation axis, (a) in the frame of zero angular momentum observers orbiting at constant radius; (b) in the frame of freely falling observers. In the panel (b), two regions of ingoing/outgoing lines are distinguished by different levels of shading of the horizon. The hole rotates counter-clockwise ($a = M$).

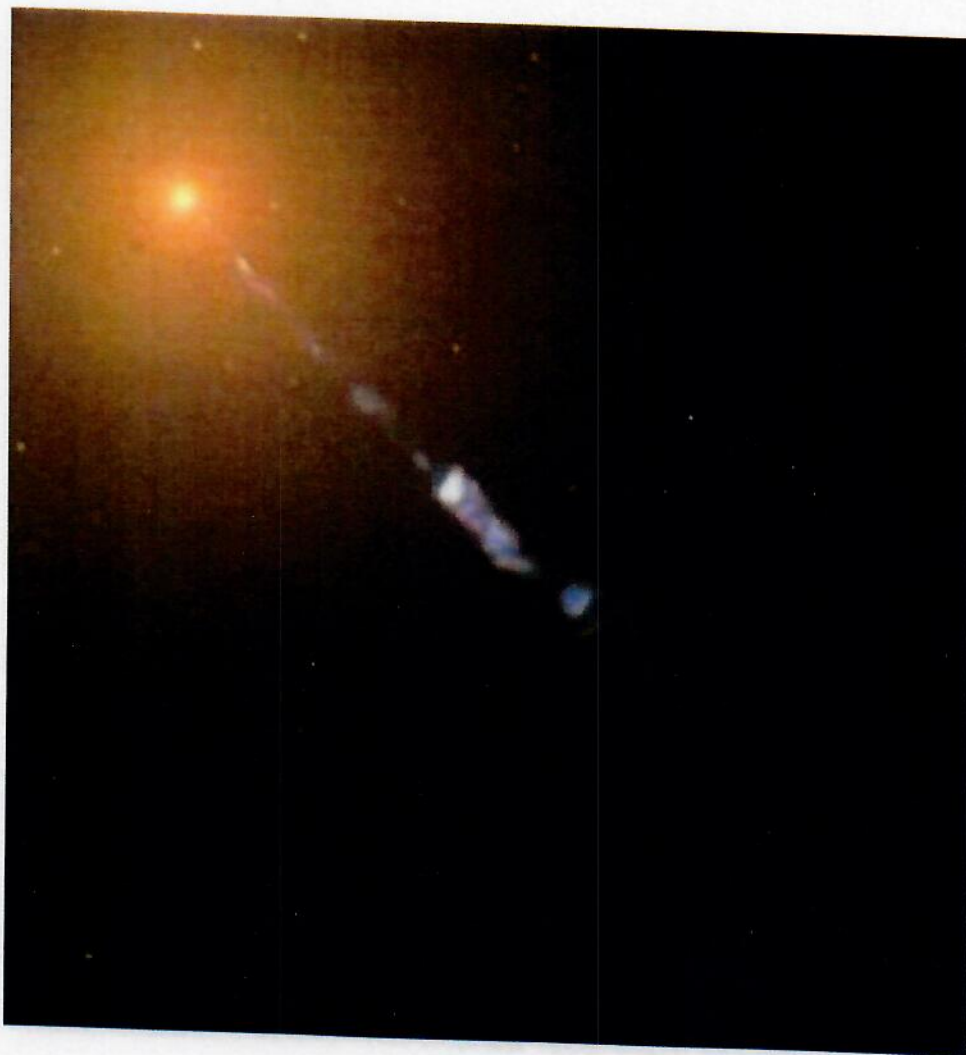
$$\Phi = 0: \Phi = B_0 \pi r_+^2 \left(1 - \frac{a^2}{r_+^2}\right), \quad r_+ = M + \sqrt{M^2 - a^2}$$

$$\Phi \neq 0: \forall |a| \leq 1 \exists \delta_{\max} \Rightarrow \Phi_{\max} \quad (a = M \Rightarrow \delta_{\max} \sim -63^\circ, \phi \sim 2.25 B_1 \pi r_+^2)$$

From: J. Bičák, V. Karas & T. Ledvinka: "Black holes and magnetic fields" in "Black Holes from Stars to Galaxies - Across the Range of Masses," ed. V. Karas, G. Matt, Cambridge University Press 2007



Structure of magnetic field lines close to a rotating black hole. Field lines in the equatorial plane. Color indicates intensity of the field. Horizon is in the center as a point. Critical point in the \rightarrow direction where field vanishes. Field lines are dragged by rotation in vacuum (no conductive medium around).



Jet from the nucleus of the elliptic galaxy M87
 moving with $v \sim c$, ^{Around} ~~In the~~ center shining stars (not individually
 distinguishable). In the center rotating supermassive black hole
 (photograph from the Hubble telescope).

Mass of M87 $\approx 200 M_{\text{our galaxy}}$

Near-horizon structure of escape zones of electrically charged particles around weakly magnetized rotating black hole: Case of oblique magnetosphere

Vladimír Karas¹ | Ondřej Kopáček^{1,2}

¹Astronomical Institute, Czech Academy of Sciences, Prague, Czech Republic

²Faculty of Science, Humanities and Education, Technical University of Liberec, Liberec, Czech Republic

Correspondence

Vladimír Karas, Boční II 1401, CZ-14100 Prague, Czech Republic.
Email: vladimir.karas@cuni.cz

Funding information

Czech Ministry of Education, Youth and Sports COST program, Grant/Award Number: LTC 18058; Czech Science Foundation, Grant/Award Number: 19-01137J

Abstract

We study the effects of large-scale magnetic fields on the dynamics of charged particles near a rotating black hole. We consider a scenario in which the initially neutral particles on geodesic orbits in the equatorial plane become ionized, and hence they are destabilized by the charging process. Fraction of charged particles are then accelerated out of the equatorial plane and then follow jet-like trajectories with relativistic velocities. We explore nonaxisymmetric systems in which the magnetic field is inclined with respect to the black hole spin. We study the system numerically in order to locate the zones of escaping trajectories and compute the terminal escape velocity. By breaking the axial symmetry, we notice increasing fraction of unbound orbits which allow for acceleration to ultrarelativistic velocities.

KEYWORDS

accretion, accretion disks, black hole physics, chaos, magnetic fields, relativity

1 | INTRODUCTION

Nuclei of many galaxies are thought to harbor supermassive black holes. Strong gravity is manifested by a variety of effects, ranging from very rapid motion of stars in dense nuclear clusters, shape of broadened skewed spectral lines from gaseous accretion disks, and other indirect evidence (Bambi 2016; Haardt et al. 2016). Furthermore, electromagnetic field plays an important role in shaping the gaseous structures and accelerating particles in the immediate vicinity of black holes in active galaxies (Klein & Fletcher 2015; Meier 2012). The system can be described by a set of mutually coupled Einstein-Maxwell equations within the framework of General Relativity.

Although the presence of supermassive, strongly gravitating, dark compact objects is indicated by numerous

independent approaches, the individual pieces of evidence for the black hole event horizon are challenging and not unique; new progress is expected with the help of multi-messenger observations in the near future (see Mészáros et al. 2019, and further references cited therein).

Mathematically rigorous and astrophysically relevant solution is defined with great precision by Kerr metric (Carter 1971; Kerr 1963), where only the mass and angular momentum are free parameters that characterize the black hole and need to be measured by observation. Cosmic black holes are surrounded by gaseous environment and embedded in magnetic fields of external origin which are both essential for the process of mass accretion and light emission, however, these two ingredients have very little impact on resulting form of the gravitational field unless the black hole forms a compact binary system, in

which case the dynamical space-time emerges and gravitational waves are released – we do not consider the latter possibility in the present paper.

Because of high conductivity of plasma that forms accretion flows and due to strong differential rotation near the black hole, the effect of even weak electromagnetic fields is crucial. Near the equatorial plane, within the accretion torus, magnetic fields are turbulent and entangled on small-length scales ℓ (less than the geometrical thickness of the disk, $\ell \lesssim h(R)$); this leads to effective viscosity and drives the accretion process (Balbus & Hawley 1991). On the other hand, in relatively empty funnels near the rotation axis, magnetic lines become organized on large scales (exceeding gravitational radius, $\ell \gtrsim R_g$); this accelerates some plasma in collimated jets away from the black hole, so that only a small fraction of accreted material plunges into the event horizon (Tchekhovskoy et al. 2011). However, details of the mechanism responsible for this acceleration and collimation still remain a matter of debate (Rezzolla & Zanotti 2013).

In Kopáček & Karas (2018), we studied the role of a large-scale magnetic field aligned with the rotation axis of a rotating black hole. We assumed that an equatorial accretion disk orbits the black hole down to the innermost stable circular orbit (ISCO, originally called the marginally stable orbit by Bardeen et al. (1972) and we explored the process of acceleration of electrically charged particles from the disk plane. In particular, we were interested in the terminal velocity that particles can reach under astrophysically realistic intensity of the aligned magnetic field (a few $\times 10^2$ gauss), and we found that the magnetic acceleration does operate, however, the particles typically reach only moderate Lorentz factors, $\gamma \lesssim 3$. We also found that the regular (non-chaotic, integrable) motion typical for particles near an unperturbed (vacuum) black hole is broken; the imposed component of the external magnetic field leads to the emergence of zones of chaotic motion. Furthermore, in Kopáček & Karas (2020) we relaxed the assumption of axial symmetry of the magnetic field and we studied the acceleration and chaoticity of motion by the magnetic field inclined with respect to the rotation axis. Interestingly, the oblique component leads to a more efficient acceleration and a larger terminal velocity, and a more complex (fractal) structure of the zones of chaotic motion. Let us emphasize that a combination of magnetic acceleration with the frame dragging by the black hole angular momentum are important. This happens because both the motion of particles as well as the shape of the magnetic field lines are affected by rotation.

In the present contribution, we further explore how a moderately inclined magnetic field influences the terminal acceleration as a function of the black hole spin parameter ($|a| \leq 1$). We concentrate our attention to the case of

co-rotation, $a > 0$, and we focus on small radii, where the General Relativity effects operate most prominently. An interesting aspect of the adopted scenario is the fact that the acceleration process is most efficient in the vicinity of the plunging region boundary. It can thus be expected that the ejected particles form a hollow structure, which only further out spreads into a uniform collimated jet or an outflow. To this end, the chaotic character of the outgoing trajectories enhances the mixing.

2 | EJECTION OF CHARGED PARTICLES FROM MAGNETIZED ERGOSPHERE

The spacetime metric coefficients of the Kerr black hole can be written in the well-known Boyer-Lindquist coordinate system (Chandrasekhar 1983; Misner et al. 1973; Wald 1984). The metric obeys the axial symmetry about the rotation axis and stationarity with respect to time, with a singularity hidden below the event horizon, where the curvature rises above all limits. Far from the event horizon, at spatial infinity the spacetime becomes asymptotically flat. All its mass M is thus concentrated in the origin. The only other free parameter a of the Kerr metric describes its rotation; the condition about the presence of the outer event horizon at a certain radius, $r = R_+$ (where the horizon encompasses the singularity) leads to the condition on maximum value of the dimensionless spin rate: $|a| \leq 1$. However, the case of excessive spin and the naked singularity is not a priori forbidden and the hereby described mathematical description remains in most of its aspects still valid without any change. The Kerr black hole solution can be then written in the form of the metric element (Chandrasekhar 1983; Misner et al. 1973)

$$ds^2 = -\frac{\Delta \Sigma}{A} dt^2 + \frac{\Sigma}{\Delta} dr^2 + \Sigma d\theta^2 + \frac{A \sin^2 \theta}{\Sigma} (d\phi - \omega dt)^2, \quad (1)$$

where $\Delta(r) = r^2 - 2r + a^2$, $\Sigma(r, \theta) = r^2 + a^2 \cos^2 \theta$, $A(r, \theta) = (r^2 + a^2)^2 - \Delta a^2 \sin^2 \theta$, $\omega(r, \theta) = 2ar/A(r, \theta)$ (geometrical units are assumed with the speed of light c and gravitational constant G set to unity). The above-given metric describes the vacuum spacetime, where the right-hand-side of the Einstein equations vanishes (no terms contribute to the energy-momentum tensor). This is clearly an astrophysical unrealistic assumption, nevertheless, it can be substantiated to certain precision if the amount of accreted matter is relatively small and the external electromagnetic fields are weak. Both assumptions are usually imposed, although this needs to be checked in each particular case. For example, the presence of a dense nuclear star-cluster and/or a massive accretion torus can change the gravitational field of the central

black hole significantly; moreover the infall and a merger of a secondary black hole must lead to a non-stationary situation where gravitational waves are produced and the line element of the gravitational field is very different from the Kerr metric, albeit for only a limited period of time.

Finding self-consistent solutions of mutually coupled Einstein-Maxwell fields is a difficult task because of inherent non-linearity of the problem. Only a very limited class of exact solutions have been found under the simplifying assumptions about axial symmetry and stationarity (Karas & Budínová 2000; Karas & Vokrouhlický 1991; Kramer & Schmutzer 1980); otherwise, one has to resort to numerical approaches. Fortunately, astrophysically realistic electromagnetic fields are usually weak with regard to their gravitational influence. One can thus explore test solutions of the Maxwell fields on the curved background of Kerr metric. The imposed spacetime is kept fixed, so that it does not evolve in time. Even if non-axisymmetric configurations cannot be stationary, the expected time scale of the spacetime evolution are very long. On the technical side, this assumption means that we neglect all coupling terms of higher than the second order in electric and magnetic components.

On the black hole background, the electromagnetic fields must be generated by currents flowing in the cosmic plasma far outside the event horizon. Within the limited volume around the black hole, the prevailing term corresponds to an asymptotically uniform magnetic field, which we will adopt hereafter. Even in this case, near the horizon the field line structure becomes increasingly entangled by the frame dragging Bičák & Dvořák (1976); King et al. (1975). This structure becomes even more complex once the assumption about an axial symmetry is abandoned; the twisted field lines develop magnetic null points where reconnection events can occur (see, e.g., Dovčiak et al. 2000; Karas et al. 2012). In the adopted weak electromagnetic field limit, the immediate consequence of the linearization is the fact that resulting electromagnetic four-vector can be written as a superposition of two parts $A^\mu = A_0^\mu + A_1^\mu$, the first one corresponding to an asymptotically uniform field aligned with the black hole rotation axis, and the other one corresponding to an asymptotically perpendicular configuration. Let us note that a small contribution to the black hole intrinsic electromagnetic field can originate from Kerr-Newman electric charge; however, this component is negligible due to rapid discharge by selective accretion of charged particles.

The case of uniform test magnetic field (corresponding to the aligned orientation) was first studied by Wald (1974). The magnetic field along the black hole rotation is described by two non-vanishing components of the

four-potential,

$$A_{0,t} = B_0 a [r \Sigma^{-1} (1 + \mu^2) - 1], \quad (2)$$

$$A_{0,\phi} = B_0 \left[\frac{1}{2} (r^2 + a^2) - a^2 r \Sigma^{-1} (1 + \mu^2) \right] \sigma^2, \quad (3)$$

in dimension-less spheroidal coordinates ($\mu = \cos \theta$, $\sigma = \sin \theta$). Equations (2)–(3) represent an asymptotically homogeneous magnetic field. The component perpendicular to the black hole axis has been given by Bičák et al. (2007; Bičák & Janiš (1985),

$$A_{1,t} = B_1 a \Sigma^{-1} \Psi \sigma \mu, \quad (4)$$

$$A_{1,r} = -B_1 (r - 1) \sigma \mu \sin \psi, \quad (5)$$

$$A_{1,\theta} = -B_1 \left[(r \sigma^2 + \mu^2) a \cos \psi + (r^2 \mu^2 + (a^2 - r) (\mu^2 - \sigma^2)) \sin \psi \right], \quad (6)$$

$$A_{1,\phi} = -B_1 \left[\Delta \cos \psi + (r^2 + a^2) \Sigma^{-1} \Psi \right] \sigma \mu, \quad (7)$$

where $\psi \equiv \phi + a \delta^{-1} \ln[(r - R_+)/ (r - R_-)]$, $\Psi = r \cos \psi - a \sin \psi$, $\delta = R_+ - R_-$, and $R_\pm = 1 \pm \sqrt{1 - a^2}$. An arbitrarily inclined magnetic field can be obtained as superposition of the two above-given components. Their mutual relation defines the asymptotic angle of the magnetic lines of force. The set of four-potential vector components defines the structure of the electromagnetic tensor, $F_{\mu\nu} \equiv A_{[\mu, \nu]}$.

Let us note that the adopted solution for the black hole gravitational and electromagnetic fields is a very special one. Regarding the space-time metric, two Killing symmetries are imposed (stationarity and axial symmetry) and no further material is allowed to contribute to gravity (electro-vacuum test solution). These assumptions immediately exclude any significant mass in stars and the surrounding gas, and it also ignores the curvature arising from distant cosmological terms (an asymptotically flat metric is employed). Also the electromagnetic part of the solution represents merely the first term in the multipole expansion of the general solution for weak electric and magnetic intensities, which are stationary and organized on length scales exceeding the gravitational radius (no time dependent, turbulent currents are allowed). However, we have relaxed the assumption about axial symmetry: the magnetic field at spatial infinity is inclined at an arbitrary angle with respect to the black hole rotation axis.

The present paper builds on Kopáček & Karas (2020); we proceed systematically over the range of spin values and we demonstrate how the chaos gradually emerges in the particle motion. The transition to non-integrability is an interesting effect which requires the electromagnetic acceleration; it does not occur in the case of geodesic

motion which is known to be completely integrable in Kerr metric (Kopáček & Karas 2014).

3 | MOTION WITHIN ESCAPE ZONES AND THE TRANSITION TO CHAOS

As mentioned above, we extend the numerous studies of the particle motion near black holes by considering one additional aspect that influences the trajectories in a distinct manner. This is the interplay between rotation of the black hole, as specified by the spin parameter a (dimensionless angular momentum of the black hole $-1 \leq a \leq 1$), which defines the axis of symmetry of the gravitational field and the corresponding (perpendicular) equatorial plane, and an asymptotically uniform magnetic field, which is aligned along a different (arbitrary) angle of inclination α ($\alpha = 0$ refers to the aligned configuration, whereas $\alpha = \pi/2$ the case of magnetic field perpendicular to the rotation axis). New features emerge which are not observed for particles near classical Kerr (rotating) and Kerr-Newman (rotating, electrically charged) black holes. Firstly, corridors of unbound escape motion occur for electrically charged particles that are injected into magnetospheres and start their acceleration on the fractal boundary region between plunging and bound trajectories. Secondly, these regions of chaotic motion develop where initially neighboring trajectories separate exponentially from each other, as characterized covariantly in terms of properly defined Lyapunov coefficients and Poincaré sections (and alternative signatures of chaos, such as the method of recurrence plots; Kopáček et al. 2010a, 2010b).

Two main characteristics of the black hole spacetime are the mass M and spin $a \equiv J/M^2c$, where J is the black hole angular momentum. Gravitational radius in physical units is then given by $R_g \equiv GM/c^2 \doteq 1.5 \times 10^5 M/M_\odot$ [cm], the outer horizon is located at radius $R_g (1 + \sqrt{1 - a^2})$, and the ergosphere at $R_g (1 + \sqrt{1 - a^2 \cos^2 \theta})$. Besides these canonical parameters, in our current model we have additional freedom in the above-mentioned magnetic angle α , which relates two intensity components B_0 , B_1 , and the particle specific electric charge q/m . The system thus requires to specify a set of three independent parameters to be fully defined in geometrical units.

By introducing the external electromagnetic interaction the particle motion loses integrability. In consequence, we have to resort to numerical integration which needs to be performed systematically over the entire parameter space in order to reveal the emerging islands of chaos. For the purposes of the present investigation, we start by setting the inclination angle α and magnetization

parameter qB , and we integrate the system of equations of particle motion in their Hamiltonian form (Kopáček & Karas 2020),

$$\mathcal{H} = \frac{1}{2} g^{\mu\nu} (\pi_\mu - qA_\mu) (\pi_\nu - qA_\nu), \quad (8)$$

where π_μ is the canonical momentum and $g^{\mu\nu}$ contravariant components of the metric tensor. The equations of motion then read

$$\frac{dx^\mu}{d\lambda} \equiv p^\mu = \frac{\partial \mathcal{H}}{\partial \pi_\mu}, \quad \frac{d\pi_\mu}{d\lambda} = -\frac{\partial \mathcal{H}}{\partial x^\mu}, \quad (9)$$

with $\lambda \equiv \tau/m$ being the affine parameter and τ proper time along the trajectory.

Figure 1 depicts three different types of trajectories that start from the black hole equatorial plane (x, y) at some initial radius $r = r_0$. These trajectories are distinguished into three categories according to the final fate of the particle: (i) plunging orbits which enter into the black hole horizon; (ii) stable orbits bound to the black hole while avoiding accretion; and (iii) ejected orbits along which particles can escape away from the black hole to radial infinity. Distinct features can be observed, which are obviously invariant with respect to the choice of coordinate system. Firstly, the escaping trajectories start to emerge for non-zero values of spin and they exist up to $a \rightarrow 1$. These orbits spatially occur approximately in between stable and plunging trajectories; however, the image suggests an interesting fractal structure. This would be naturally expected on the basis of the fact that some selected trajectories in the escaping region appear to be chaotic by numerical integration.

In order to reveal details of this complex region, we can zoom progressively into small parts of the phase space. An example is shown in Figure 2, where we plot the three classes of the trajectories in (a, r_0) plane. Let us note that the region of escaping orbits can come up above ISCO at certain value of $a \approx 0.5$. However, for high values of $|qB|$ the resulting escape zone can even get inside the ergosphere, although the region is then very narrow. Because the plots have been generated by numerical integration, a natural question has to be raised regarding the precision and the sensitivity to initial conditions. We integrated the motion equations in the hamiltonian form via Adams-Bashforth-Moulton multi-step integrator, as described in a recent paper (Kopáček & Karas 2020) in more detail. The routine is based on the predictor-corrector loop with the adaptive step-size and the local truncation error controlled by a relative tolerance parameter. Further, to verify the precision, we also employed Dormand & Prince explicit Runge-Kutta type scheme (ode873; Dormand & Prince 1978; Prince & Dormand 1981). Comparing the output, we conclude that

FIGURE 1 The three classes of the orbits parameterized by the black hole spin a and projected on the top view of the equatorial plane around the black hole. A hollow structure of escaping particles is visible (yellow). Color-coding: blue for plunging orbits, red for stable orbits, and yellow for escaping trajectories. The green circle denotes the innermost stable circular orbit (ISCO), which moves from $R_{\text{ISCO}}(a=0) = 6$ down to $R_{\text{ISCO}}(a=1) = 1$. The white circle is the boundary of the ergosphere. The inner black region marks the horizon of the black hole, $r = R_+(a)$. The other parameters of the system are $\alpha = 35^\circ$ and $qB = -5$. The asymptotic direction of the magnetic field is inclined in the positive x -axis direction

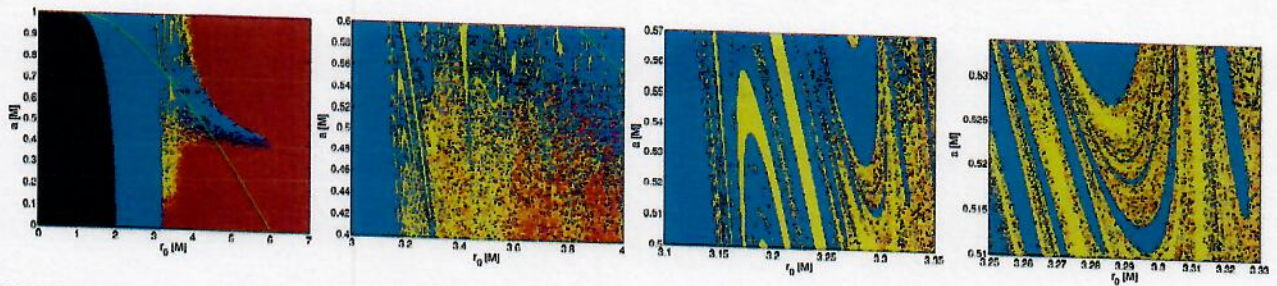
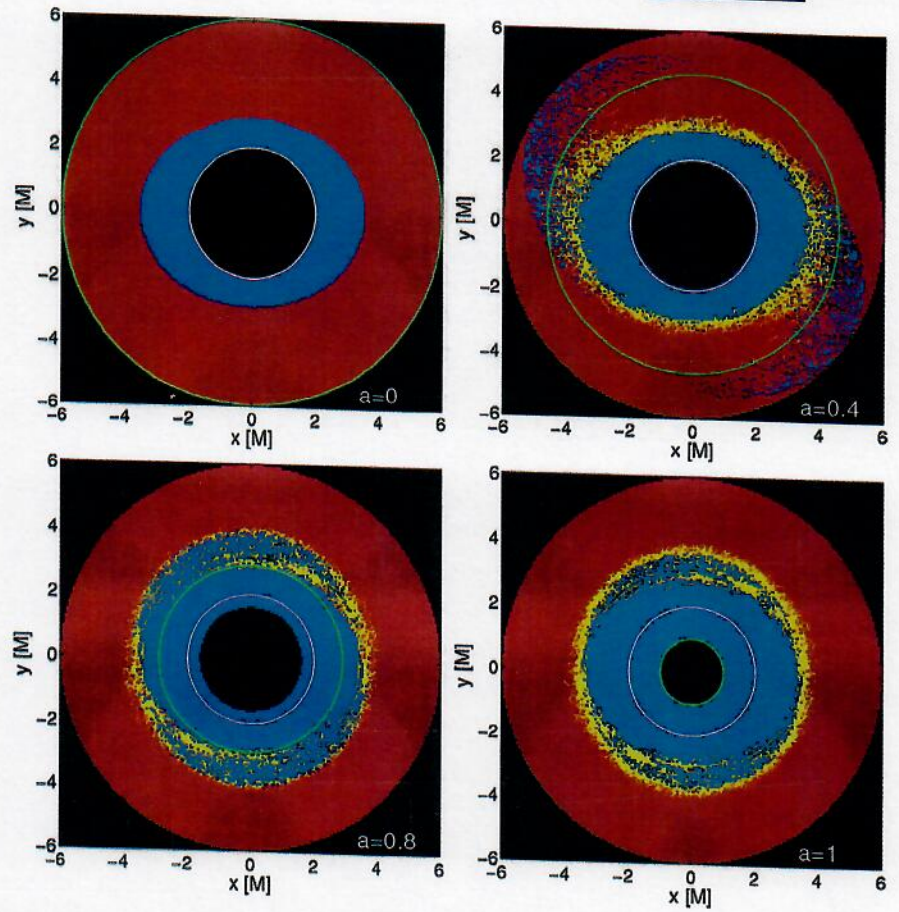


FIGURE 2 The fractal structure emerges of escaping, plunging, and bound trajectories with the rising value of spin a . Gradually increasing resolution is shown going from left to right. Parameters: $\alpha = 35^\circ$, $qB = -5$ and $\varphi_0 = 135^\circ$

the overall structure produced by the two independent schemes is consistent and the regions of different classes of trajectories agree. However, let us also note that caution always has to be paid with respect to the precision. For example, the standard fourth-order Runge–Kutta integration routines are not adequately accurate to reflect the regions of chaos (Kopáček et al. 2014).

Regarding the class of escaping trajectories an interesting question concerns the final velocity that the ejected particles can reach. To this end, we construct a color-coded map of the terminal Lorentz factor γ in Figure 3. In this particular example, we set $qB_0 < 0$ (a necessary condition for the particle escape). The main ingredients that are

necessary and sufficient to launch the outflow of charged particles are a combination of rotation of the central black hole with the imposed large-scale magnetic field. A moderately misaligned configuration increases the efficiency of acceleration. On the other hand, a perfect alignment (magnetic vector parallel with the spin, for the same values of all other parameters) restricts considerably the efficiency of the acceleration mechanisms.

The escape zone is clearly distinguished in the plot by yellow to green colors, where the acceleration reaches up to $\gamma \approx 2.5$ for the given set of other (frozen) parameters. The plots confirm that the escaping particles originate from a rather narrow range of radii between $2.5 \lesssim r \lesssim 3.5$. This

KK5

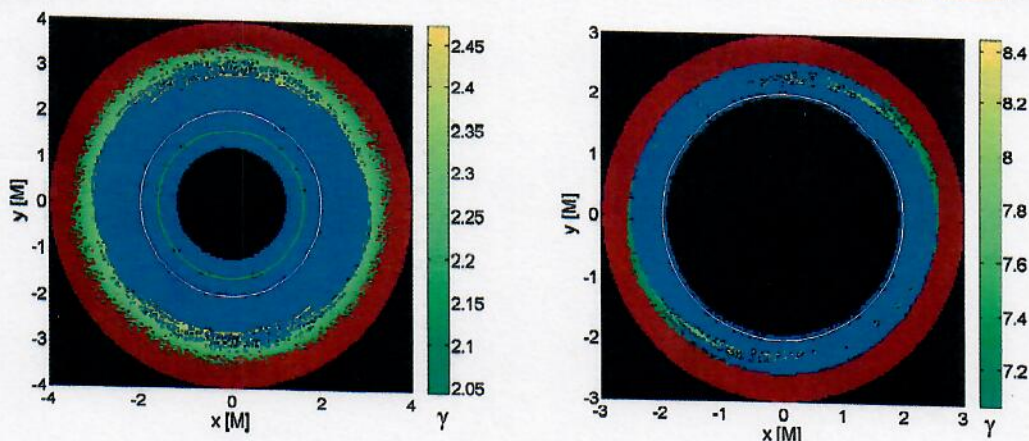


FIGURE 3 Final Lorentz factor γ of the escaping trajectories. Values of several parameters have been kept fixed. *Left panel:* moderate angle of the magnetic field $\alpha = 25^\circ$, charge and magnetization $qB = -5$, and almost maximally rotating Kerr hole $a = 0.98$. *Right panel:* $\alpha = 35^\circ$, $qB = -50$, $a = 0.4$

is a generic picture which appears typically for moderate $\alpha \lesssim 45^\circ$. On the other hand, for $\alpha \gtrsim 45^\circ$ we found that the particles can escape from only certain azimuthal locations (for further details, see also Kopáček & Karas 2020).

4 | DISCUSSION AND CONCLUSIONS

We further examined aspects of charged particle acceleration in the region of organized magnetic field near rotation axis of Kerr black hole. While the magnetic field develops a prevailing toroidal component in the equatorial torus, where they are highly turbulent, in the diluted above the torus the large-scale poloidal field lines help to accelerate a stream of outflowing particles which eventually form a collimated jet. This picture has been suggested by several independent numerical simulations Rezzolla et al. (2011). It turns out that a moderate (non-zero) inclination of the large-scale magnetic field helps the acceleration; the effect operates less efficiently in the axially symmetric (aligned, $\alpha \rightarrow 0$) configuration, and it is also less efficient in the highly inclined (or even perpendicular, $\alpha \rightarrow \pi/2$) case. We find that the ejection mechanism requires an interplay between rotation of the black hole and the magnetic field. The particles originate from the region in the equatorial plane near above the outer boundary of the ergosphere and below the innermost stable circular orbit, therefore very close to the horizon.

The ejection region exhibits fractal structure and the trajectories show signatures of chaos. Although we had to resort to numerical integration of the trajectories, we verified the precision of our method by employing two highly accurate schemes and checking the results independently by recurrence analysis; all approaches qualitatively agree.

The emergence of chaos is an interesting feature in the black hole spacetime, where the orbits of the unperturbed Kerr metric are known to be fully integrable. Although any direct observation confirmation about the character of motion is difficult or impossible because of an insufficient resolution, it is interesting to recall the hollow structure of the wobbling jet in the core of M87 elliptical galaxy (Britzen et al. 2017; Hada et al. 2016). Here, the resolution of the interferometric images reaches down to the horizon scale, and it indeed appears that the material of the jet might start from around the inner rim of the accretion torus, corresponding to the region indicated by the ejected (yellow) orbits in our graphs.

ACKNOWLEDGMENTS

We thank the Czech Science Foundation, grant ref. 19-01137J and the Czech Ministry of Education, Youth and Sports COST program ref. LTC 18058 to support international collaboration in relativistic astrophysics.

REFERENCES

Balbus, S. A., & Hawley, J. F. 1991, *Astrophys. J.*, 376, 214.
 Bambi, C. 2016, *Astrophysics of Black Holes*, Vol. 440, Springer-Verlag (Berlin).
 Bardeen, J. M., Press, W. H., & Teukolsky, S. A. 1972, *Astrophys. J.*, 178, 347.
 Bičák, J., & Dvořák, L. 1976, *Gen. Relat. Gravitat.*, 7(12), 959.
 Bičák, J., & Janiš, V. 1985, *MNRAS*, 212, 899.
 Bičák, J., Karas, V., & Ledvinka, T. 2007, in: *Black Holes from Stars to Galaxies—Across the Range of Masses*, eds. V. Karas & G. Matt, Vol. 238, Cambridge University Press (Cambridge), 139.
 Britzen, S., Fendt, C., Eckart, A., & Karas, V. 2017, *Astron. Astrophys.*, 601, A52.
 Carter, B. 1971, *Phys. Rev. Lett.*, 26, 331.
 Chandrasekhar, S. 1983, *The Mathematical Theory of Black Holes*, Oxford University Press (Oxford).
 Dormand, J. R., & Prince, P. J. 1978, *Celest. Mech.*, 18(3), 223.

- Dovčiak, M., Karas, V., & Lanza, A. 2000, *Eur. J. Phys.*, 21(4), 303.
- Haardt, F., Gorini, V., Moschella, U., Treves, A., & Colpi, M. 2016, *Astrophysical Black Holes*, Vol. 905, Taylor & Francis Group (New York).
- Hada, K., Kino, M., Doi, A., et al. 2016, *Astrophys. J.*, 817(2), 131.
- Karas, V., & Budínová, Z. 2000, *Phys. Scr.*, 61(2), 253.
- Karas, V., & Vokrouhlický, D. 1991, *J. Math. Phys.*, 32(3), 714.
- Karas, V., Kopáček, O., & Kunneriath, D. 2012, *Class. Quant. Grav.*, 29(3), 035010.
- Kerr, R. P. 1963, *Phys. Rev. Lett.*, 11(5), 237.
- King, A. R., Lasota, J. P., & Kundt, W. 1975, *Phys. Rev. D*, 12(10), 3037.
- Klein, U., & Fletcher, A. 2015, *Galactic and Intergalactic Magnetic Fields*. Heidelberg, New York, Springer Praxis Books, Springer International Publishing.
- Kopáček, O., & Karas, V. 2014, *Astrophys. J.*, 787(2), 117.
- Kopáček, O., & Karas, V. 2018, *Astrophys. J.*, 853(1), 53.
- Kopáček, O., & Karas, V. 2020, *Astrophys. J.*, 900(2), 119.
- Kopáček, O., Karas, V., Kovář, J., & Stuchlík, Z. 2010a, *Astrophys. J.*, 722(2), 1240.
- Kopáček, O., Kovář, J., Karas, V., & Stuchlík, Z. 2010b, *Recurrence Plots and Chaotic Motion around Kerr Black Hole*. M. de León, D. M. de Diego, & R. M. Ros (Eds.), Am. Inst. Phys. Conf. Ser. Vol. 1283, p. 278. Melville (NY), American Institute of Physics.
- Kopáček, O., Karas, V., Kovář, J., & Stuchlík, Z. 2014, Proc. RAGTime 10–13: Workshops Black Holes Neutron Stars, p. 123. Silesian University, Opava.
- Kramer, D., & Schmutzer, E. 1980, *Exact Solutions of Einstein's Field Equations*, Cambridge University Press (Cambridge).
- Meier, D. L. 2012, *Black Hole Astrophysics: The Engine Paradigm*, Springer (Berlin).
- Mészáros, P., Fox, D. B., Hanna, C., & Murase, K. 2019, *Nat. Rev. Phys.*, 1(10), 585.
- Misner, C. W., Thorne, K. S., & Wheeler, J. A. 1973, *Gravitation*, W. H. Freeman (San Francisco).
- Prince, P. J., & Dormand, J. R. 1981, *J. Comp. Appl. Math.*, 7(1), 67.
- Rezzolla, L., & Zanotti, O. 2013, *Relativistic Hydrodynamics*, Oxford University Press (Oxford).
- Rezzolla, L., Giacomazzo, B., Baiotti, L., Granot, J., Kouveliotou, C., & Aloy, M. A. 2011, *Astrophys. J. Lett.*, 732(1), L6.
- Tchekhovskoy, A., Narayan, R., & McKinney, J. C. 2011, *MNRAS*, 418(1), L79.
- Wald, R. M. 1974, *Phys. Rev. D*, 10, 1680.
- Wald, R. M. 1984, *General Relativity*, Chicago University Press (Chicago).

AUTHOR BIOGRAPHY

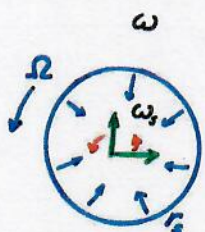
Vladimir Karas is professor of astrophysics and the current managing director of the Astronomical Institute of the Czech Republic (since 2012). He leads the Relativistic Astrophysics Working Group, which he had established in the Prague section of the Institute in 2004. Previously he held research and teaching positions at Charles University and elsewhere. Over the years Vladimir has supervised students at various levels and he has served at professional committees and panels. He has developed novel fast numerical approaches to examine effects of strong gravity via light variations from sources near a black hole (e.g. Karas et al., Monthly Notices of the Royal Astronomical Society, Vol. 259, 569–575, 1992). His more recent work deals with signatures of frame-dragging in magnetic field lines, where he has an active collaboration with researchers at University of Cologne, Università Roma Tre, Silesian University in Opava, and at Polish Academy of Sciences in Warsaw. He has been co-PI of Albert Einstein Center of Theoretical Physics and Astrophysics in Prague. Vladimir contributes to the Czech participation in the upcoming eXTP satellite mission and CTA observatory.

How to cite this article: Karas V, Kopáček O. Near-horizon structure of escape zones of electrically charged particles around weakly magnetized rotating black hole: Case of oblique magnetosphere. *Astron. Nachr.* 2021;342:357–363. <https://doi.org/10.1002/asna.202113934>

Instantaneous Inertial Frames & Retarded Electromagnetic Fields in Relativistic Collapse with Rotation

Kato, Lyden-Bell, Bi., CQG

Extending & generalizing Lindblom & Brill (Phys. Rev. D 1974) (see also H. Pfister, Ch. Khin, etc.)



$$\Omega = \frac{d\varphi_{shell}}{dt} \quad \text{small (neglect } \Omega^2 \text{)}$$

A collapsing spherical shell (of dust) in slow rotation produces a slightly perturbed Schwarzschild spacetime outside the shell $r \geq r_s$ (in $\{t, r, \theta, \varphi\}$ coordinates):

$$ds^2 = \left(1 - \frac{2M}{r}\right) dt^2 - \frac{1}{1 - \frac{2M}{r}} dr^2 - r^2 d\theta^2 - r^2 \sin^2\theta (d\varphi - \omega dt)^2 \quad (1)$$

PERTURBATION (L=1, odd parity):

$$\omega(r) = \frac{2J}{r^3}$$

(small) fixed total angular momentum

perturbation: frame-dragging potential

Insight into Inside $\equiv \omega[\bar{t}(t)] = \frac{2J}{[r_s(t)]^3}$

$$(\omega) \quad d\bar{\varphi} = d\varphi - \omega_s dt$$



Local inertial frames (LIFs) inside ($\bar{\varphi} = \text{const}$) all rotate rigidly with the same angular velocity w.r.t. to observers at rest relative to infinity ($\varphi = \text{const}$)... "static obs.":

$$\frac{d\bar{\varphi}}{dt} = 0 \quad \Rightarrow \quad \boxed{\frac{d\varphi}{dt} = \omega_s} \quad \omega_s(t)$$

As measured in LIF's own proper time the rate of rotation is

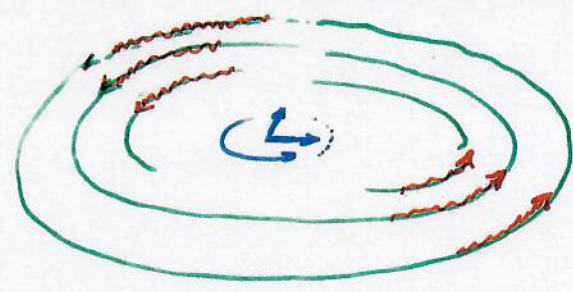
$$\frac{d\varphi}{d\bar{t}} = \bar{\omega}_s = \omega_s \frac{dt}{d\bar{t}} \Big|_s$$

Static observers inside experience Euler acceleration (their Coriolis and centrifugal $\sim \bar{\omega}_s^2$) and the congruence of their world lines twists

**Gravitational waves
and dragging effects**

2 papers in CQG 2008 (e.g. K, DLB) 2010
 yr 2000 (di Biagi, de Felice, Herrera, Valiente, Tucker)
 gyroscopes (spinning particles)
 immersed directly in a gravit. wave

We wish to tackle a more fundamental question:
*Whether energy and angular momentum
 in purely vacuum spacetimes can cause
 the local inertial frames to rotate*



If yes, is this effect, instantaneous
 as in case of rotating matter?

- Corvino & Schoen (2006) "analytic gluing technique"
 Kerr → WAVES - Kerr metric

Rotating gravitational waves in the symmetry reduced GR

pure waves, no string, only $\partial/\partial z$ symmetry,
not cylindrical ($\partial/\partial \varphi$) symmetry

$$ds^2 = e^{-2\psi} g_{ab} dx^a dx^b - e^{2\psi} dz^2$$

$\psi(x^c), g_{ab}(x^c)$ $a, b, c \dots 0, 1, 2$ ³

$\begin{matrix} \uparrow & \uparrow & \uparrow \\ t & \varphi & \psi \end{matrix}$

$$R_{ab} = 0 \Rightarrow \mathcal{R}_{ab} = 2\partial_a \psi \partial_b \psi$$

$$R_{33} = 0 \Rightarrow g^{ab} \nabla_a \nabla_b \psi = 0$$

$\mathcal{R}_{ab} \dots$ Ricci of 3 space $g_{ab} dx^a dx^b$
In 3 dimensions \mathcal{R}_{abcd} determined by \mathcal{R}_{ab}
(so here by ψ):

$$\mathcal{R}_{abcd} = 2 \left[(\mathcal{R}_{a[c} - \frac{1}{4} g_{a[c} \mathcal{R}]) g_{d]b} \right. \\ \left. - (\mathcal{R}_{b[c} - \frac{1}{4} g_{b[c} \mathcal{R}]) g_{d]a} \right]$$

1 Killing only \rightarrow 'formidable task'

\rightarrow assume ψ and derivatives small
develop approximation procedure

$$\psi = \epsilon \Psi(x^i) \rightarrow R_{ab} \sim O(\epsilon^2), R_{abcd} \sim O(\epsilon^4)$$

\rightarrow may write

$$g_{ab} = \eta_{ab} + \epsilon^2 \gamma_{ab}(x^i), \quad g^{ab} = \eta^{ab} - \epsilon^2 \gamma^{ab}$$

So we can construct a genuinely rotating
(ψ -dependent) solution of the wave eq.

in flat space and still satisfy Field Eqs.

in terms $\sim O(\epsilon^2)$ by solving $\mathcal{L}_{ab} = 2 \nabla_a \psi \nabla_b \psi$
 $\Rightarrow g_{ab} = g_{ab}(t, r, \varphi)$.

However, we are primarily interested in the
rotation of inertial frames ('gyros') at the
axis (which is regular) - φ -dependent terms in ω
do not affect the rotation there

\Rightarrow concentrate on the axially symm. terms
in the Fourier expansion of ω as function of φ
 \Rightarrow solve equations for g_{ab} averaged over φ

$$\Rightarrow \mathcal{R}_{ab} = 2 \underbrace{\langle \partial_a \psi \partial_b \psi \rangle}_{= S_{ab}} = 2 \int_0^{2\pi} \partial_a \psi \partial_b \psi d\varphi$$

So source axisymmetric, hence also g_{ab}
but $\partial\psi$ not hypersurface orthogonal

$$\left| ds^2 = e^{2\delta} (dt^2 - d\rho^2) - W^2 (d\varphi - \omega dt)^2 \right|$$

(*) no problem at the axis (like matter cyl.) dragging

$$g(t, \rho), \quad W(t, \rho) = \rho + \epsilon^2 \omega(t, \rho)$$

ϵ will be 'absorbed'

Left h. sides

EFEs: $\mathcal{R}_{00} = -\ddot{g} + \dot{g}' + \frac{1}{\rho} \dot{\rho}' - \frac{1}{\rho} \ddot{W}$

$$\mathcal{R}_{11} = \ddot{g} - \dot{g}'' + \frac{1}{\rho} \dot{\rho}'' - \frac{1}{\rho} W''$$

$$\mathcal{R}_{01} = \frac{1}{\rho} \dot{g}' - \frac{1}{\rho} \dot{W}'$$

$$\mathcal{R}_{22} = \rho (\ddot{W} - W'')$$

$$\mathcal{R}_{02} = \frac{1}{2\rho} (\rho^2 \dot{\omega}')'$$

constraint eq.

$$\mathcal{Q}_{12} = \frac{1}{2} \rho^2 \dot{\omega}'$$

Inertial frame rotation induced by rotating gravitational waves

Two equations considered explicitly:

$$\text{WE: } \ddot{\psi} - \psi'' - \frac{1}{\rho} \psi' - \frac{1}{\rho^2} \partial_\varphi^2 \psi = 0 \quad (1)$$

$$\mathcal{R}_{02} = 2S_{02}: \quad \frac{1}{2\rho} (\rho^3 \langle \omega \rangle')' = 2 \langle \dot{\psi} \partial_\varphi \psi \rangle \stackrel{+f}{=} \dot{J}_\varphi \quad (2)$$

\approx angular mom. density

Elem. Solutions of (1) expressed in Bessel functions

$$\psi = A e^{i(m\varphi - \omega t)} J_m(\omega \rho) \quad (\text{real part})$$

$\omega \neq \omega \rightarrow \omega$

$$m \neq 0 \dots \text{rotating wave: } m\varphi - \omega t = \text{const} \\ \Rightarrow \varphi = \frac{\omega}{m} t + \text{const}$$

Inspired by exact Bonnor-Weber-Wheeler pulse
take superposition (ω integrates out)

$$\psi = B \int_0^\infty (a\omega)^m e^{-a\omega} e^{i(m\varphi - \omega t)} J_m(\omega \rho) a d\omega$$

+ c.c.

$a > 0$ constant - effective duration of the pulse

Weber-Wheeler-Bonner pulse

$$ds^2 = e^{-2\psi} [e^{2\gamma} (dt^2 - dr^2) - \rho^2 d\varphi^2] - e^{2\psi} dz^2$$

$$\psi = \psi(t, r), \quad \gamma = \gamma(t, r)$$

EFEs: $\gamma' = \rho (\dot{\psi}^2 + \dot{\psi}^2), \quad \dot{\gamma} = 2\rho \dot{\psi} \psi'$

and WE: $\psi'' + \frac{1}{\rho} \psi' - \ddot{\psi} = 0$

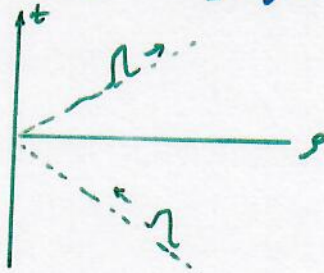
$$\tilde{\rho} = \frac{\rho}{a}, \quad \tilde{t} = \frac{t}{a}, \quad b = \frac{\sqrt{3}c}{a}$$

C, a constants

measure of the "amplitude"
the width of pulse

$$\psi = b \left\{ \frac{1 + \tilde{\rho}^2 - \tilde{t}^2 + [(1 + \tilde{\rho}^2 - \tilde{t}^2)^2 + 4\tilde{t}^2]^{1/2}}{(1 + \tilde{\rho}^2 - \tilde{t}^2)^2 + 4\tilde{t}^2} \right\}^{1/2}$$

$$\gamma = \frac{b^2}{4} \left\{ 1 - 2\tilde{\rho}^2 \frac{(1 + \tilde{\rho}^2 - \tilde{t}^2)^2 - 4\tilde{t}^2}{[(1 + \tilde{\rho}^2 - \tilde{t}^2)^2 + 4\tilde{t}^2]^2} - \frac{1 - \tilde{\rho}^2 - \tilde{t}^2}{[(1 + \tilde{\rho}^2 - \tilde{t}^2)^2 + 4\tilde{t}^2]^{1/2}} \right\}$$



Bateman Manuscript Project of Erdelyi et al
formula (8.6.5)

$$\psi = B a^{m+1} e^{im\varphi} 2^m \frac{\Gamma(m+\frac{1}{2})}{\sqrt{\pi}} \rho^m (\alpha^2 + \beta^2)^{-m-\frac{1}{2}} + c.c.$$

$$\alpha = \alpha(t) = a + it$$

Define $\tilde{\rho} = \frac{\rho}{a}, \tilde{t} = \frac{t}{a}$

use $2^m \frac{\Gamma(m+\frac{1}{2})}{\sqrt{\pi}} = (2m-1)!!$

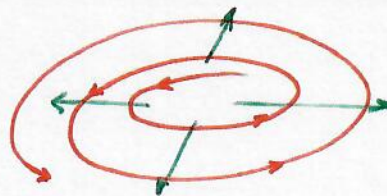
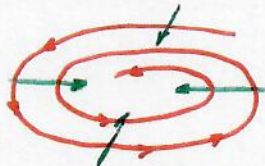
in real terms

$$\psi(\tilde{t}, \tilde{\rho}, \varphi) =$$

$$= 2B(2m-1)!! \frac{\tilde{\rho}^m \overbrace{\cos[m\varphi - (m+\frac{1}{2})\chi]}^{\text{phase}}}{[(1+\tilde{\rho}^2-\tilde{t}^2)^2 + 4\tilde{t}^2]^{\frac{1}{2}(m+\frac{1}{2})}}$$

where $\chi = \arctan \frac{2\tilde{t}}{1+\tilde{\rho}^2-\tilde{t}^2}$

$\tilde{t} \rightarrow -i\gamma$



Integrating the Einstein eq. for ρ_{00} , ω

$$\langle \omega \rangle = \frac{1}{2} \int \frac{1}{\tilde{\rho}^2} \left[\int_{\tilde{\rho}^2}^{\tilde{\rho}^2} \tilde{\rho}^2 d\tilde{\rho}^2 \right] d\tilde{\rho}^2$$

$\leftarrow -2 \langle \psi \partial_y \psi \rangle$

! integrating by parts ...

$$\langle \omega \rangle = \frac{2B^2}{a} m [(2m-1)!!]^2 \times$$

$$\times \left[\frac{m}{u} I_{m-1} + 2(2m+1) \frac{\tilde{t}^2}{u} I_m + (m-1) H_{m-1} + 2(2m+1) \tilde{t}^2 H_m \right]$$

$$I_m(u) \equiv \int_0^u u^m Q^{-m-\frac{3}{2}} du$$

$$H_m(u) \equiv \int_u^\infty u^{m-1} Q^{-m-\frac{3}{2}} du$$

$$u \equiv \tilde{\rho}^2, \quad Q = (1+u-\tilde{t}^2)^2 + 4\tilde{t}^2$$

Evaluation of $I_m(u)$, $H_m(u)$

... detailed Appendix in QGS

Rotation of inertial frames at small and great distances

On axis

$$\langle \omega \rangle_0 = \frac{B^2 (2m)!}{a 2^{2m-1}} \frac{1+m(1+\tilde{r}^2)}{(1+\tilde{r}^2)^2} \Big|_{\tilde{r}^2=0}^{+\infty}$$

Greatest at $\tilde{r} = 0$

No time lag between the wave arriving closest to the axis

- most of the energy never gets nearer than $\tilde{r} \approx 0.4$

⇒ like with the shell rotating and collapsing - non-local effect given by the constraint equation instantaneous

Far from the axis

$$\langle \omega \rangle \approx \frac{B^2 m (m!) (2m-1)!!}{a 2^{m-1}} \frac{1}{\tilde{r}^2}, \quad \tilde{r} \gg 1$$

Due to the rotation of IF rod at the origin ^{18°} points towards

$$\begin{aligned} \phi(t) &= \phi_0 + \int_{-\infty}^t \langle \omega \rangle_0 dt \\ &= \phi_0 + B^2 \frac{(2m+1)!}{2^{2m}} \left[\arctan \tilde{t} + \frac{\pi}{2} + \frac{\tilde{t}}{(2m)(1+\tilde{t}^2)} \right] \end{aligned}$$

can choose $= 0$ at $t=0$

$$\begin{aligned} \langle \omega \rangle &\approx \langle \omega \rangle_0 \left[1 - \frac{(2m-1)!!}{(m+1)!} \frac{1}{(1+\tilde{t}^2)^{m+1}} \times \right. \\ &\quad \left. \times \frac{(2m-5) + (2m+3)\tilde{t}^2}{(m+1) + m\tilde{t}^2} \left(\frac{\tilde{t}^2}{1+\tilde{t}^2} \right)^m \right] \end{aligned}$$

very small at $\tilde{t} \ll 1, m$ high like shell

Metric at $\tilde{t}^2 \ll (1+\tilde{t}^2)$

$$ds^2 \approx e^{2\psi} [dt^2 - d\rho^2 - \rho^2 (d\varphi - \langle \omega \rangle_0 dt)^2 - c^2 dx^2]$$

$\psi \sim \tilde{t}^m$ very small

in rotating axes $\tilde{\varphi} = \varphi - \phi(t)$: $ds^2 = e^{2\psi} (dt^2 - d\rho^2 - \rho^2 d\tilde{\varphi}^2) - c^2 dx^2$

flat in the reduced space

ψ at different times

Class Quantum Grav 25 (2008) 165018

D Lynden-Bell et al

18**

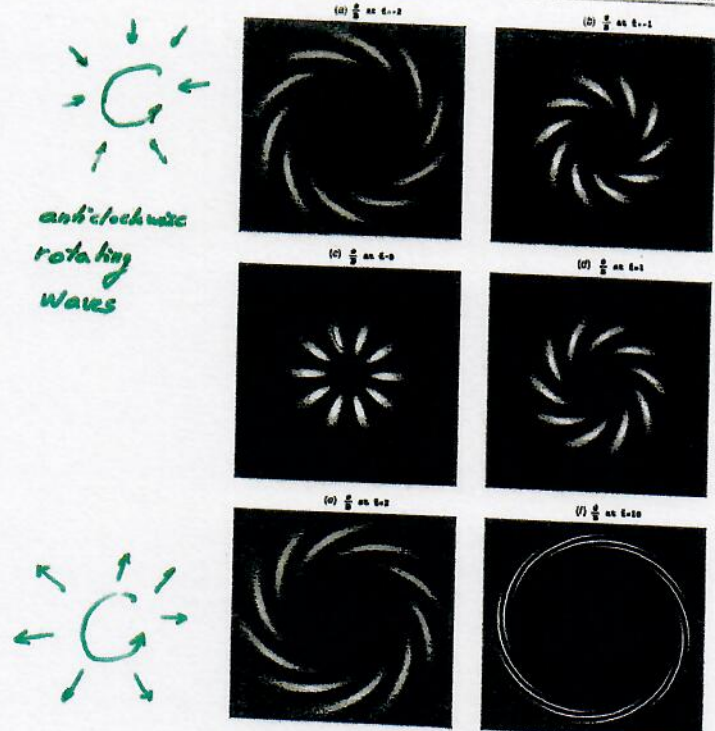


Figure 2. This shows the $m = 10$ wave which always rotates anticlockwise. As it comes inwards (a) at $t = -2$ it is in the form of a leading spiral with the outer parts of the arms ahead of the central parts. By $t = -1$ (b) the spiral has started to open. By $t = 0$ (c) the central parts have caught up and the spiral has changed to a cartwheel structure but rotation keeps it beyond $\beta \approx 0.4$. By $t = 1$ (d) the spiral has become trailing as befits a wave that now feeds angular momentum outwards. By $t = 2$ (e) the spiral becomes tighter and the flat central cylinder becomes larger. We show $t = 10$ (f) at a small scale but note the beautiful tight wrapping of the narrow arms. Also note the opposite spirality of the conjugate pairs $l = \pm 2$ and $l = \pm 1$. Figures encompass a radius $\beta \approx 7$ ($\beta \approx 17$ for $l = 10$). The height of ψ/β reduced by a factor of 10^{-4} is between 0 and 1. Lighting falls at 45° from the left. The view is along the z axis from above at a distance of $10^{-4}\psi/\beta = 40$.

orientation of rod at the origin:

$$\phi(t) = \phi_0 + \int_{-\infty}^t \langle \omega \rangle_0 dt = \dots \text{explicitly known}$$

Angular momentum transport by gravitational torques

analogy with angular momentum transport in spiral galaxies

classical gravitational stress tensor is

$$\sigma_{kl} = \frac{1}{\kappa} (2 \partial_k \psi \partial_l \psi - \rho_{lm} \sum_m |\partial_m \psi|^2)$$

ψ - is now classical gravitational potential



Gravitational couple transferring angular momentum outwards a cylinder is

$$C_{grav} = \int \epsilon_{3ke} X^k \sigma^{em} dS_m$$

↑ radius vector
↓ stress tensor


↑ outward pointing surface element

$$\Rightarrow C_{grav} = \frac{2}{\kappa} \int \partial_\phi \psi \partial_\phi \psi \rho d\phi dz$$

to carry angular momentum outwards must be a positive correlation between $\partial_\phi \psi$ and $\partial_\phi \psi$ averaged over the cylinder \Rightarrow

Trailing sense of spirality to contours of $\psi = const.$:
 outer parts of spiral galaxy trail inner parts in the sense of rotation.

Similarly with gravitational waves:
 for angular momentum transport outward,
 the spiral formed by contours of ψ must
 trail the inner parts but oppositely when
 they form a leading spiral with the outside
 further advanced than the inside and
 the angular momentum is transported inward
 (upper part of Fig.)

At $t = 0$ no angular momentum transport
 \Rightarrow contours of ψ form a rotating cartwheel
 with no spirality (Figure)

The waves themselves never reach
 much further than $\tilde{r} = 1$ (flat space around
 axis). But
 the 2nd order effect of the angular
 momentum causes the rotation of
 the inertial frame within the waves

L

ROTATING SCALAR WAVES

In linear analysis one can use simple prescription

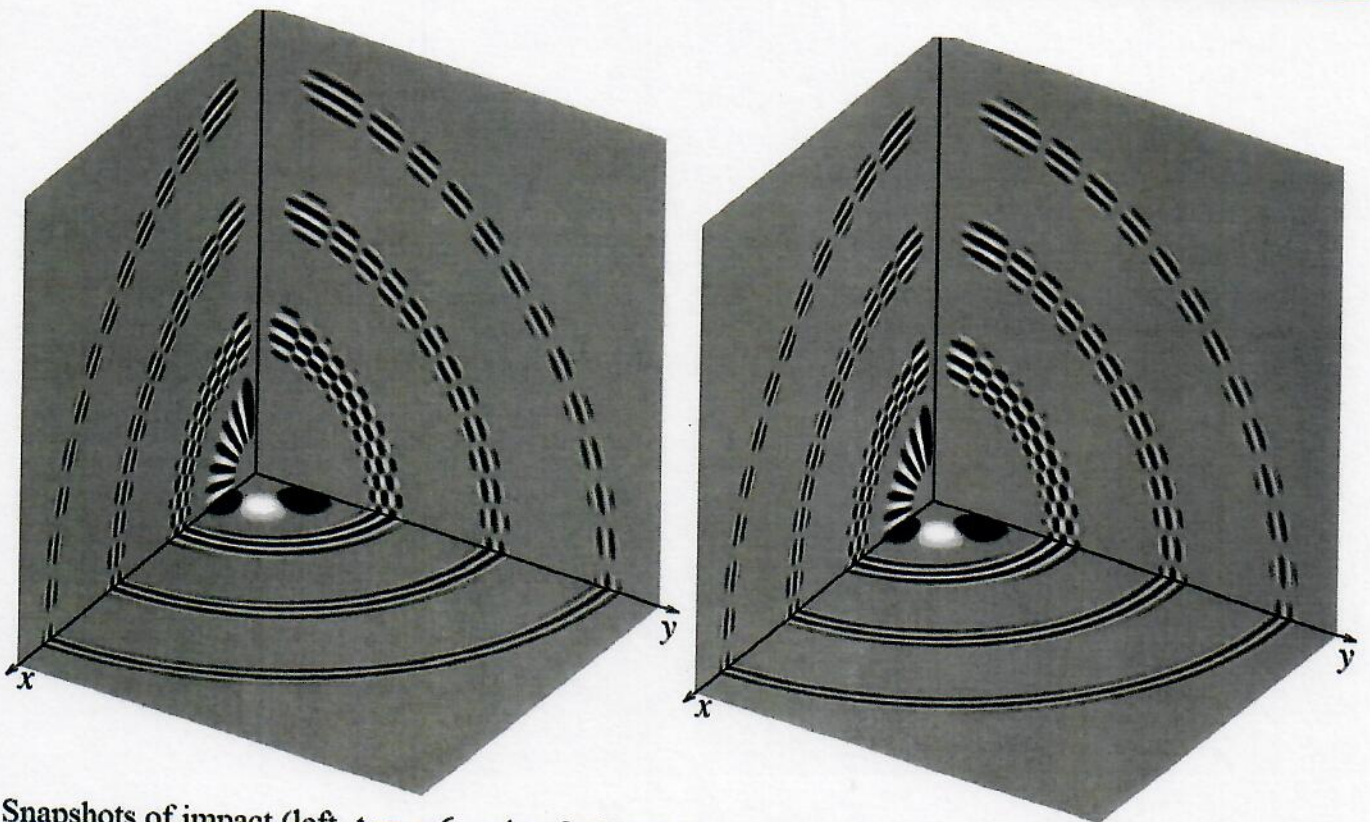
$$\psi_{lm}(t, r, \theta, \phi) \sim \operatorname{Re} \frac{\left(\frac{r}{a}\right)^l}{\left[\frac{(a+it)^2+r^2}{a^2}\right]^{l+1}} Y_{lm}(\theta, \varphi) e^{-i\omega t}$$

In nonlinear terms, we may need an explicit form

$$\psi_{lm}(t, r, \theta, \phi) \sim \frac{\left(\frac{r}{a}\right)^l}{\left[\frac{(a^2+r^2-t^2)^2+4a^2t^2}{a^4}\right]^{\frac{l+1}{2}}} P_l^m(\cos \theta) \cos(m\phi - \lambda(t, r))$$

$$\lambda(t, r) = (l+1) \arctan \frac{2at}{a^2 + r^2 - t^2}$$

ROTATING SCALAR WAVES



Snapshots of impact (left, $t = -6, -4, -2, 0$) and departure (right, $t = 0, 2, 4, 6$) of scalar spherical version of Weber-Wheeler-Bonnor pulse with $l = 27, m = 5$.

ROTATING LINEARIZED GRAVITATIONAL WAVES

Expansion of (odd parity) symmetric second-rank covariant tensor into tensor harmonics

$$h_{\mu\nu}^{(i)} = \sum_{lm} \frac{\sqrt{2l(l+1)}}{r} \left[-h_{0lm}^{(i)}(t, r) c_{0lm\mu\nu} + ih_{1lm}^{(i)}(t, r) c_{1lm\mu\nu} + \frac{i\sqrt{(l-1)(l+2)}}{2r} h_{2lm}^{(i)}(t, r) d_{1lm\mu\nu} \right],$$

$$c_{0lm} = \frac{r}{\sqrt{2l(l+1)}} \begin{pmatrix} 0 & 0 & \frac{1}{\sin\theta} \partial_\varphi Y_{lm} & -\sin\theta \partial_\theta Y_{lm} \\ 0 & 0 & 0 & 0 \\ \frac{1}{\sin\theta} \partial_\varphi Y_{lm} & 0 & 0 & 0 \\ -\sin\theta \partial_\theta Y_{lm} & 0 & 0 & 0 \end{pmatrix},$$

$$c_{1lm} = \frac{ir}{\sqrt{2l(l+1)}} \begin{pmatrix} 0 & 0 & 0 & 0 \\ 0 & 0 & \frac{1}{\sin\theta} \partial_\varphi Y_{lm} & -\sin\theta \partial_\theta Y_{lm} \\ 0 & \frac{1}{\sin\theta} \partial_\varphi Y_{lm} & 0 & 0 \\ 0 & -\sin\theta \partial_\theta Y_{lm} & 0 & 0 \end{pmatrix},$$

SECOND-ORDER ODD PARITY DIPOLE PERTURBATIONS

Now we have solved the first order Einstein equations

$$G_{\mu\nu}^{(1)}[h^{(1)}] = 0$$

In general the second-order metric perturbations $h^{(2)}$ can be obtained by solving

$$G_{\mu\nu}^{(1)}[h^{(2)}] = -G_{\mu\nu}^{(2)}[h^{(1)}, h^{(1)}],$$

right-hand side is the source term in the form of an effective energy-momentum tensor

$$G_{\mu\nu}^{(1)}[h^{(2)}] = -\frac{1}{2} \left[h_{\mu\nu}^{(2); \alpha} + h_{\mu\alpha}^{(2); \nu} + h_{\nu\alpha}^{(2); \mu} - h_{\alpha}^{(2); \mu\nu} - \bar{g}_{\mu\nu} \left(h_{\beta\alpha}^{(2); \alpha\beta} - h_{\beta}^{(2); \beta; \alpha} \right) \right].$$

Rotation $\phi' = \phi - \omega_0 t \rightarrow ds^2 = \dots + r^2 \sin^2 \theta (d\phi - \omega_0 dt)^2$ is most easily identified in

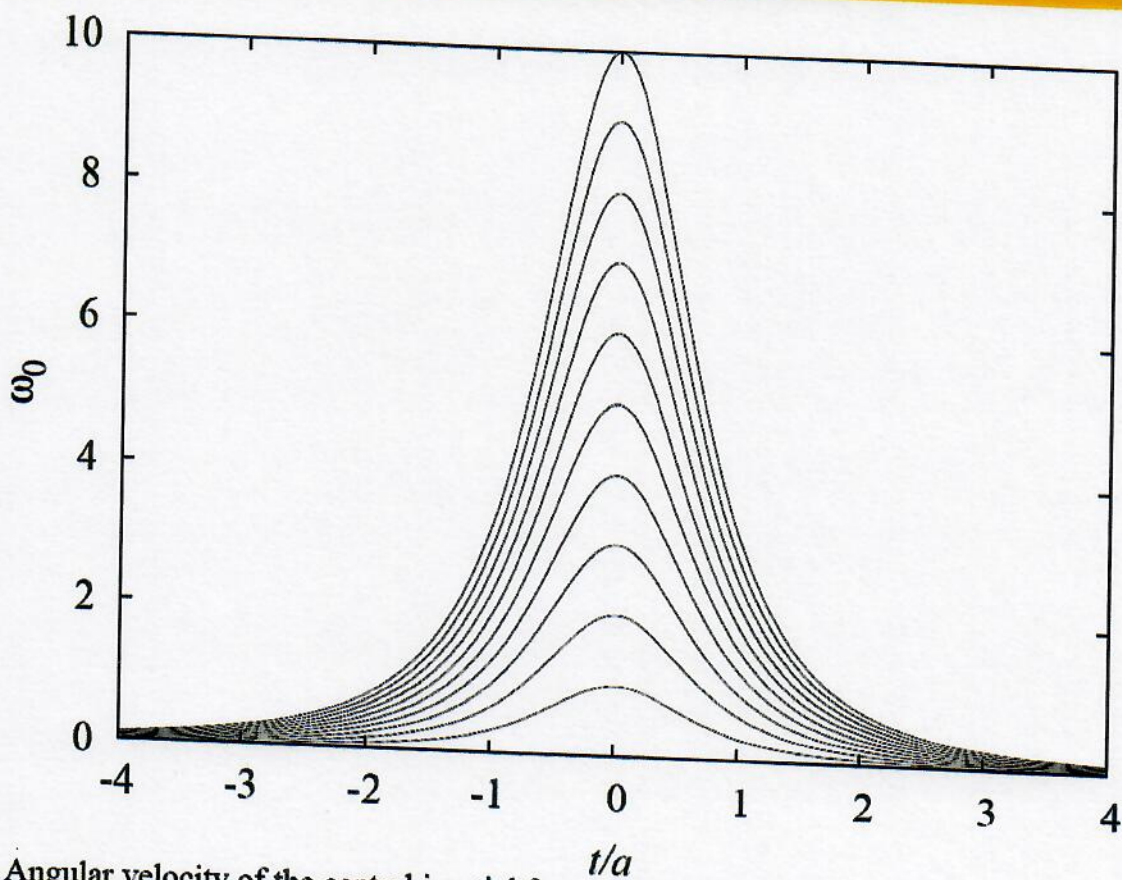
$$g_{t\phi}^{(2)} = -\omega_0 r^2 \sin^2 \theta$$

since $t\phi$ -component is associated only with the following tensor harmonic component

$$c_{0lm} r_\phi = \frac{r}{\sqrt{2l(l+1)}} (-\sin \theta \partial_\theta Y_{lm})$$

the dragging of inertial frames near the origin is given by $l = 1, m = 0$ perturbation

CENTRAL INERTIAL FRAME DRAGGING



Angular velocity of the central inertial frame $\omega_0(l, m; t)$ for $l = 10$ and $m = 1, 2, \dots, 10$. The vertical axis is scaled in units of $\omega_0(10, 1; 0)$.

By Mach's principle we mean:

" all motions, velocities, rotations and accelerations are relative; local inertial frames are determined through the distributions of energy and momentum in the Universe by some weighted averages of the apparent motions "

H. Bondi, Cosmology 1952

We show how such averages are to be taken for perturbed FLRW universes and demonstrate "Mach" for the spherical universes

PHYSICAL REVIEW D 76, 063501 (2007)

Cosmological perturbation theory, instantaneous gauges, and local inertial frames

Jiří Bičák

*Institute of Theoretical Physics, Faculty of Mathematics and Physics, Charles University,
V Holešovičkách 2, 180 00 Prague 8, Czech Republic and Max Planck Institute for Gravitational Physics, Albert Einstein Institute,
Am Mühlenberg 1, D-14476 Golm, Germany*

Joseph Katz

Racah Institute of Physics, Hebrew University, Jerusalem 91904, Israel

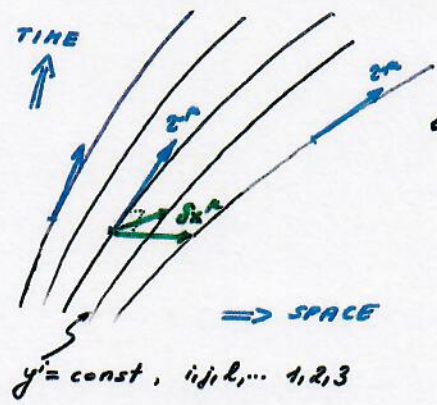
Donald Lynden-Bell

*Institute of Astronomy, The Observatories, Madingley Road, Cambridge CB30HA, United Kingdom
(Received 26 July 2006; revised manuscript received 28 June 2007; published 5 September 2007)*

Linear perturbations of Friedmann-Robertson-Walker universes with any curvature and cosmological constant are studied in a general gauge without decomposition into harmonics. Desirable gauges are selected as those which embody best Mach's principle: in these gauges local inertial frames can be determined instantaneously via the perturbed Einstein field equations from the distributions of energy and momentum in the universe. The inertial frames are identified by their "accelerations and rotations" with respect to the cosmological frames associated with the "Machian gauges." In closed spherical universes, integral gauge conditions are imposed to eliminate motions generated by the conformal Killing vectors. The meaning of Traschen's integral-constraint vectors is thus elucidated. For all three types of Friedmann-Robertson-Walker universes the Machian gauges admit much less residual freedom than the synchronous or generalized harmonic gauge. Mach's principle is best exhibited in the Machian gauges in closed spherical universes. Independent of any Machian motivation, the general perturbation equations and discussion of gauges are useful for cosmological perturbation theory.

Cosmological perturbation theory,
 "NACHMAN"
 instantaneous gauges & local inertial frames

- General spacetime (universe)



filled with
 cosmological
 observers' (frames)
 COFs
 congruence of COs:
 $x^\mu = x^\mu(y^i; p)$
 $\mu = 0, 1, 2, 3$

τ^μ ... unit, timelike - 4-velocity of CO (are "Lie propagated")

$\delta x_{(i)l}^\mu = P_{ij}^\mu \frac{\partial x^\nu}{\partial y^j}$... connecting vectors
 spacelike, $\perp \tau^\mu$
 projection $\perp \tau^\mu$
 if 3 indep. unit: $\{m_{ij}^\mu\}$

Decomposition of $\tau_{\mu;\nu}$

$\tau_{\mu;\nu} = \tau_\nu \alpha_\mu + \omega_{\mu\nu} + \sigma_{\mu\nu} + \frac{1}{3} \theta P_{\mu\nu}$

acceleration vorticity (rotation) shear expansion
 i.e. $\theta = \tau^\mu{}_{;\nu}$

from now on:

Linearly perturbed FRW models

$g_{\mu\nu} = \bar{g}_{\mu\nu} + h_{\mu\nu}$ $\tilde{h}_{\mu\nu}$ if $dt = a(t)dy$
 $d\tilde{s}^2 = dt^2 - a^2(t) f_{nc}(x^a) dx^k dx^l$ "conformal time"

e.g. $d\tilde{s}^2 = dt^2 - a^2(t) [dx^2 + \sum_k (d\theta_k^2 \sin^2 \theta d\phi^2)]$



perturbed $k=+1$

$\Sigma_k = \begin{cases} \sin \chi & k=+1 \quad S^3 \\ \chi & k=0 \quad E^3 \\ \sinh \chi & k=-1 \quad H^3 \end{cases}$

Now find:

vorticity $\omega_{nc} = \delta \omega_{nc} = \frac{1}{2} (h_{0k,l}^{\cdot} - h_{0l,k}^{\cdot})$
shear $\sigma_{nc} = \delta \sigma_{nc} = \frac{1}{2} \dot{h}_{nc} - \frac{1}{6} \dot{h}_m^m \bar{g}_{nc} - \frac{a}{2} \dot{h}_{nc}$
 ($\omega_{0n} = \delta \omega_{0n} = \sigma_{0n} = \delta \sigma_{0n} = 0$)

Expansion

$\theta = \bar{\theta} + \delta\theta = \frac{3\dot{a}}{a} + \frac{1}{2} (\dot{h}_m^m - \frac{3\dot{a}}{a} h_0^0 - \nabla_n h_0^0)$

background

The accelerations of COFs w.r.t. LIFs
(i.e. "accel." of LIFs w.r.t. COFs - mutually
at rest...)

$$\boxed{\alpha_\mu = \tau_{\mu\nu} \tau^\nu} \leftarrow \text{general, covariant form}$$

In perturbed FRW

$$\boxed{\alpha^\ell = \bar{g}^{\ell m} \left(-\frac{1}{2} h_{00,m} + \dot{h}_{0m} \right)}$$

↑
in Newtonian limit $\nabla\Phi$

Summary: in perturbed FRW universes,
to determine rotation and acceleration
of Local Inertial Frames we need to
know $\boxed{h_{00,e} \quad h_{0b,m} \quad \dot{h}_{0e}}$

TASKS: - can these ↑ be determined
instantaneously from matter variables $\rho T_{\mu\nu}$,
possibly $\rho \dot{T}_{\mu\nu}$? (ρT_{00} , ρT_{0i} , ρT_{0e})
- how uniquely in different types
of universes? (S^3 , E^3 , H^3 , ... richer topologies)

conformal time $dt = a(\eta)d\eta$
 $a(\eta)$... expansion factor $\mathcal{H} = \frac{a'}{a} = \mathcal{H}a$ $\dot{\eta} = \frac{d}{d\eta}$

Einstein Field Equations for perturbations

$\tilde{h}_{T^k}^l = \tilde{h}_k^l - \delta_k^l \tilde{h}_n^n$ *general gauge
no harmonics
no decompositions*

et

$T_k = \nabla_l \tilde{h}_{T^k}^l$, $\mathcal{K} = \frac{3}{2} a \dot{h}_{00} + \frac{1}{2} a \dot{h}_n^n - \nabla_k \tilde{h}_k^k$

follows Einstein's perturbation equations, separating δ_k^l , the traceless part from the trace $\delta \tilde{G}_n^n$ which we combine with $\delta \tilde{G}_0^0$ for a reason to be seen below, defining $\nabla^2 = f^{kl} \nabla_{kl}$, we have the following dimensionless equations

$$\begin{aligned}
 a^2 \kappa \delta \tilde{T}_0^0 &= a^2 \delta \tilde{G}_0^0 = \nabla^2 \tilde{h}_n^n + k \tilde{h}_n^n - 2\mathcal{H}\mathcal{K} - \nabla_k T^k, \\
 a^2 \kappa \delta \tilde{T}_k^0 &= a^2 \delta \tilde{G}_k^0 = \nabla^2 \tilde{h}_{k0} + k \tilde{h}_{k0} + \nabla_{kl} \tilde{h}_0^l \\
 &\quad + \nabla_k \mathcal{K} - (T_k)^{\dots}, \\
 a^2 \kappa (\delta \tilde{T}_0^0 - \delta \tilde{T}_n^n) &= a^2 (\delta \tilde{G}_0^0 - \delta \tilde{G}_n^n) = \nabla^2 \tilde{h}_{00} \\
 &\quad + 3a \left(\frac{1}{a} \mathcal{H}\right)' \tilde{h}_{00} + \frac{2}{a} (a\mathcal{K})', \\
 \text{and finally} \\
 a^2 \kappa (\delta \tilde{T}_k^l - \delta_k^l \delta \tilde{T}_n^n) &= a^2 \delta_k^l = -\nabla^2 \tilde{h}_{T^k}^l + k \tilde{h}_{T^k}^l + \frac{1}{2a^2} \left[a^2 \left(\frac{\tilde{h}_k^l}{T^k}\right)' \right] \\
 &\quad + f^{lm} (\nabla_{(m} T_{k)} - f_{mk} \nabla_n T^n) \\
 &\quad - \frac{1}{a^2} f^{lm} \left[a^2 (\nabla_{(m} \tilde{h}_{k)0} - f_{mk} \nabla_n \tilde{h}_0^n) \right]' \\
 &\quad + f^{lm} (\nabla_{mk} - f_{mk} \nabla^2) (\tilde{h}_{00} - \tilde{h}_n^n).
 \end{aligned}$$

in the case of perfect fluid perturbations with local coordinate velocity compo

$\tilde{v}^k = \frac{dx^k(\eta)}{d\eta}$

have

$a^2 \kappa \delta \tilde{T}_0^0 = a^2 \kappa \delta \rho$, $a^2 \kappa \delta \tilde{T}_k^0 = 2(k + \mathcal{H}^2 - \mathcal{H}')(-\tilde{v}_k + \tilde{h}_{k0})$,

Instantaneous ("Machian") gauges in cosmology

Mach 1, Mach 2, 2*, Mach 3, 3*
 differences in the time slicing of a
perturbed universe, i.e. in the choice
 of time coordinate (possible changes by $f^{(i)}$)
 i.e. in the choice of "snapshot"



The choice of spatial coordinates on given
 slices the same in all Machian gauges

$$(*) \quad \mathcal{G}_k = \nabla_{\ell} \tilde{h}_{\ell k} = 0 \quad \tilde{h}_{\ell k} = h_{\ell k} - \frac{1}{3} \delta_{\ell k} h^m_m$$

$k, \ell, \dots = 1, 2, 3$ spatial only

motivated by non-linear GR, numerical relativity
 "minimal-distortion shift vector" (Smarr...)

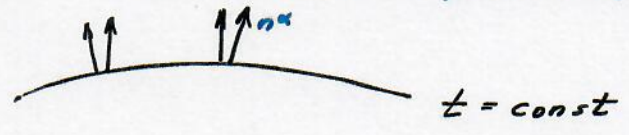
In Schwarzschild (for slicings \perp geodesics from ∞)

$$ds^2 = (1 - 2M/r) dt^2 - 2\sqrt{\frac{2M}{r}} dr dt - dr^2 - r^2(d\theta^2 + \sin^2\theta d\varphi^2)$$

Mach 1

(*) + constant mean ^{extrinsic} curvature slicing
(GR, QG, ...)

↔ uniform Hubble expansion (Bordean)



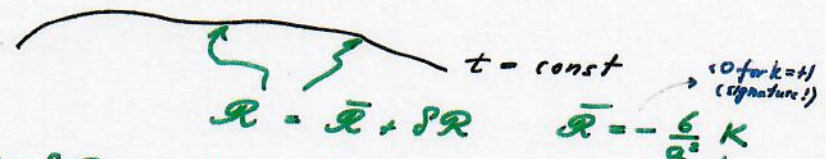
$\delta n^\alpha{}_{;\alpha} = 0 \rightarrow$

$\mathcal{K} = \frac{3}{2} \dot{a} \tilde{h}_{00} + \frac{1}{2} a \dot{\tilde{h}}^m_m - \mathcal{P} = 0$

$\mathcal{P} = \nabla_e \tilde{h}_0^e \quad (= f(t))$

Mach 2

(*) + constant mean intrinsic (scalar) curvature slicing



$\mathcal{R} = \bar{\mathcal{R}} + \delta \mathcal{R} \quad \bar{\mathcal{R}} = -\frac{6}{a^2} K$

$0 = \delta \mathcal{R} = -\frac{2}{3a^2} (\nabla^2 \tilde{h}^m_m + 3K \tilde{h}^m_m) + \frac{1}{a^2} \nabla_m \mathcal{G}^m$

$\underbrace{\quad}_{=0}$

6746



REMBRANDT FAUST

- References on Mach's principle, gravomagnetic effects and related questions
- [1] E. Mach: Die Mechanik in ihrer Entwicklung : historisch-kritisch dargestellt. Brockhaus, Leipzig 1883. (English edition: The Science of Mechanics, A Critical and Historical Account of Its Development, 6th edition. Open Court Publishing, La Scalle, IL 1960.
- [2] A. Einstein: „Gibt es eine Gravitationswirkung die der elektromagnetischen Induktionswirkung analog ist?“, Vierteljahrschrift für gerichtliche Medizin (ser. 3), 44, 37–40 (1912).
- [3] H. Pfister: „On the history of the so-called Lense-Thirring effect“, Gen. Rel. Grav. 39 1735–1748 (2007).
- [4] C. W. F. Everitt et al: „Gravity Probe B test of general relativity“, Class. Quantum Grav. 32 224001 (2015).
- [5] V. Karas, O. Kopáček, D. Kunneriath: „Influence of frame-dragging on magnetic null points near rotating black holes“, Class. Quantum Grav. 29, 35109 (2012); see also the original review: J. Bičák, V. Karas: „The influence of black holes on uniform magnetic fields“, in Proceedings of the 5th M. Grossmann Meeting, eds. Blair D.G. and Buckingham M.J., World Scientific, Singapore 1989, Vol. 2, 1999-1207.
- [6] J. Bičák: „Machian aspects of the present-day cosmology“, in Ernst Mach and the Development of Physics, edited by V. Prosser and J. Folta. Universitas Carolina Pragensis Press, Prague, 1991. There are also contributions by J. Barbour, J. Ehlers, F. Embacher, H. Pfister, G. Holton and others.
- [7] H. Bondi: „Cosmology“, Cambridge University Press, Cambridge 1961.
- [8] Mach's Principle: From Newton's Bucket to Quantum Gravity, edited by J. Barbour and H. Pfister, Einstein studies Vol. 6. Birkhäuser, Boston, 1995).

- [9] D. Lynden-Bell, J. Katz, J. Bičák: „Mach's principle from the relativistic constraint equations”, Mon. Not. R. Astron. Soc. 272, 150-160 (1995), Errata: MN 277, 1600 (1995).
- [10] J. Katz, D. Lynden-Bell, J. Bičák: “Instantaneous Inertial Frame but Retarded Electromagnetism in Rotating Relativistic Collapse”, Class.Quant.Grav. 15 (1998) 3177-3194
- [11] D. Lynden-Bell, J. Bičák, J. Katz: “On Accelerated Inertial Frames in Gravity and Electromagnetism”, Annals Phys. 271 (1999) 1-22.
- [12] T. Doležal, J. Bičák, N. Deruelle: “Slowly rotating voids in cosmology”, Class.Quant.Grav. 17 (2000) 2719-2737
- [13] J. Bičák, D. Lynden-Bell, J. Katz: “Do Rotations Beyond the Cosmological Horizon Affect the Local Inertial Frame?” Phys.Rev. D69 (2004) 064011 (12 pp).
- [14] J. Bičák, J. Katz, and D. Lynden-Bell, “Cosmological perturbation theory, instantaneous gauges and local inertial frames”, Phys. Rev. D 76, 063501 (2007) (31pp).and references by the same authors therein.
- [15] J. Bičák, J. Katz, and D. Lynden-Bell: „Gravitational waves and dragging effects”, Class. Quantum Grav. 25, 165017 (2008) (19pp); D. Lynden-Bell, J. Bičák, and J. Katz, „Inertial frame rotation induced by rotating gravitational waves” Class. Quantum Grav. 25, 165018 (2008) (13pp); J. Bičák, J. Katz, and D. Lynden-Bell: “Effects of rotating gravitational waves”, Phys. Rev. D 85, 124003 (2012) (16pp).